Dynamical Model of Coherent Pion Production in Neutrino-Nucleus Scattering

S. X. Nakamura,[1,*] T. Sato,[2] T.-S. H. Lee,[3] B. Szczerbinska,[4] and K. Kubodera[5]

[1]*Instituto de Física, Universidade de São Paulo, C.P. 66318, 05315-970, São Paulo, SP, Brazil*

[2]*Department of Physics, Osaka University, Toyonaka, Osaka, 560-0043, Japan*

[3]*Physics Division, Argonne National Laboratory, Argonne, Illinois 60439, USA*

[4]*Dakota State University, College of Arts & Sciences, Madison, SD, 57042-1799, USA*

[5]*Department of Physics and Astronomy, University of South Carolina, Columbia, SC, 29208, USA*

(Dated: October 6, 2009)

Abstract

We study coherent pion production in neutrino-nucleus scattering in the energy region relevant to neutrino oscillation experiments of current interest. Our approach is based on a combined use of the Sato-Lee model of electroweak pion production on a nucleon and the Δ-hole model of pion-nucleus reactions. Thus we develop a model which describes pion-nucleus scattering and electroweak coherent pion production in a unified manner. Numerical calculations are carried out for the case of the ^{12}C target. All the free parameters in our model are fixed by fitting to both total and elastic differential cross sections for $\pi-^{12}$C scattering. Then we demonstrate the reliability of our approach by confronting our prediction for the coherent pion photo-productions with data. Finally, we calculate total and differential cross sections for neutrino-induced coherent pion production, and some of the results are (will be) compared with the recent (forthcoming) data from K2K, SciBooNE and MiniBooNE. We also study effect of the non-locality of the Δ-propagation in the nucleus, and compare the elementary amplitudes used in different microscopic calculations.

PACS numbers: 13.15.+g, 14.60.Pq, 25.30.Pt

Keywords: neutrino-nucleus scattering, neutrino oscillation, pion production

*Electronic address: satoshi@jlab.org; Current affiliation: Excited Baryon Analysis Center (EBAC), Thomas Jefferson National Accelerator Facility, Newport News, VA 23606, USA

I. INTRODUCTION

The detailed theoretical study of neutrino-nucleus reactions is of great current importance due to the ever increasing precision of neutrino oscillation experiments (recently carried out, on-going and forthcoming). Since most of these experiments measure the neutrino flux through neutrino-nucleus scattering, reliable theoretical estimates of the relevant cross sections are prerequisite for the accurate interpretation of the data. Some of these experiments (T2K, MiniBooNE, etc.) use neutrinos in an energy range within which the dominant processes are the quasi-elastic nucleon knockout and the quasi-free single-pion production through the excitation of the Δ (1232) resonance. Meanwhile, coherent single-pion production in this energy region (albeit not a dominant process) is also of considerable interest, since it allows us to study, with no ambiguity concerning the final nuclear state, the details of the Δ-excitation mechanism and medium effects on the pion; the knowledge of these details is essential for predicting the dominant quasi-free pion production processes. In this paper we focus on the coherent single-pion production process.

There have indeed been quite active experimental efforts to investigate neutrino-induced coherent single-pion production in the Δ-excitation region. K2K[1] and SciBooNE[2] investigated charged-current (CC) coherent pion production, while MiniBooNE[3] studied neutral-current (NC) coherent pion production. Furthermore, results for the anti-neutrino-induced coherent pion-production processes are expected to become available soon from MiniBooNE for the NC process [4], and from SciBooNE for the CC process [5]. It is to be remarked, however, that the recent experimental results offer a rather puzzling situation. The experiments at K2K[1] and SciBooNE[2] report that the CC process is not observed, whereas the MiniBooNE experiment [3] concludes that the NC process is observed. Now, from the isospin factors, we expect an approximate relation $\sigma_{CC} \sim 2\sigma_{NC}$. Although the muon mass can reduce the phase space for the CC process at low energies, we still expect that σ_{CC} should be of a significant size compared with σ_{NC}, and hence the above experimental results seem quite puzzling. In this connection it is to be noted that the MiniBooNE's use of the Rein-Sehgal (RS) model [6] in analyzing the NC data has recently be questioned [7]: for a critical review of the RS model, see Refs. [7, 8]. The CC data analyses in Refs.[1, 2] did not rely on a particular theoretical model for coherent pion production itself but, in dealing with some other neutrino-nucleus reactions that entered into the analyses, certain models whose reliability was open to debate needed to be invoked.

The theoretical treatment of coherent pion production can be categorized into two types: a PCAC-based model and a microscopic model. In the former approach, the hadronic matrix element for neutrino-induced pion production is related to the pion-nucleus (or pion-nucleon) scattering amplitude through the PCAC relation. Meanwhile, in the microscopic approach, the hadronic matrix element is calculated by summing the elementary amplitude for weak

pion-production off a single nucleon embedded in a nuclear environment.

A prominent example of the PCAC-based approach is the model due to Rein and Sehgal (RS model) [6]. Because of its success in the high energy neutrino process [9] ($E_\nu \gtrsim 2$ GeV, where E_ν is the incident neutrino energy) and its simplicity, the RS model has been extensively used in analyzing data in neutrino-oscillation experiments. Several authors, however, have recently pointed out that the RS model does not give a reasonable description for relatively low-energy neutrino processes ($E_\nu \lesssim 2$ GeV)[7, 8], and that the use of the RS model may have led to the puzzling experimental situation currently facing us. There have been several proposals [8, 10, 11, 12] to remedy some of the possible insufficiencies in the original RS model.

Meanwhile, in order to build a quantitatively reliable microscopic approach, it is obviously of primary importance to start with a model that can describe with sufficient accuracy electroweak pion production off a free single nucleon. Furthermore, for pion production off a nuclear target, we need to consider medium effects such as the final-state interactions (FSI) between the outgoing pion and nucleus, etc. Recently there have been several microscopic calculations[7, 13, 14, 15], the most elaborate one being that by Amaro et al. [7]. These calculations differ in the way the elementary process ($\nu_\mu N \to \mu^+ N\pi$) is modeled and/or in the way the medium effects are taken into account. For example, only the resonant Δ-excitation mechanism is considered in Refs. [13, 14], while the non-resonant mechanism is additionally considered in Refs. [7, 15]. It was shown in Refs. [7, 15] that the inclusion of the non-resonant mechanism leads to a reduction of the cross section by a factor of ~ 2, even though both models are constructed in such a manner that the data for the elementary process are reproduced fairly well. [1] This result indicates the importance of modelling the elementary process with a sound and systematic approach which has been extensively tested by available data.

The purpose of the present article is to develop an alternative microscopic model for coherent pion production. An important ingredient of our formalism is a reliable dynamical model for the elementary process, and for that we shall employ the Sato-Lee (SL) model [16, 17]. The SL model was first developed as a systematic framework for studying the resonance properties by analyzing data on pion production in photon (electron)-nucleon scattering in the Δ-resonance region [16, 18]. The SL model treats the resonant and non-resonant mechanisms on the same footing, and is known to provide a reasonably accurate description of an extensive set of pion production data. The SL model was further extended to the weak sector in Ref. [17], and was shown to be able to reproduce data for neutrino-induced pion production off a nucleon. As has been done in the previous microscopic calculations,

[1] Unfortunately, conclusive data for the elementary neutrino process are still lacking, which leads to theoretical uncertainty.

we also need to incorporate the nuclear medium effects. In the energy region of our interest, the Δ-hole approach has proved to be successful in describing various processes involving pion-nucleus dynamics. These situations motivate us to develop a model for coherent pion production by combining the SL model and the Δ-hole model, and this is what we attempt in this article. We shall limit ourselves here to a case where the target nucleus (and hence the final nucleus also) has spin 0, and employ a simplified Δ-hole model proposed in Ref. [19]. As for concrete numerical calculations, we concentrate on the ^{12}C target, which has been and will continue to be an important nuclear target in many of neutrino-oscillation experiments. To test the reliability of our approach, we first calculate observables for coherent photo-pion production on ^{12}C using the same theoretical framework and show that the calculated results agree well with data. We then proceed to calculate observables for coherent neutrino-pion production on ^{12}C and present numerical results that can be compared with the recent data from K2K and SciBooNE. We shall also present theoretical predictions for those quantities for which experimental data will soon become available.

The fact that the previous microscopic calculations exhibit rather large model-dependence makes it particularly interesting to use the SL model, which has been highly successful in the single nucleon sector. The SL model provides a consistent set of amplitudes for pion production and pion-nucleon scattering on a single nucleon; all these amplitudes are obtained in a systematic manner from the same Lagrangian. In our approach this consistency can be further taken over to the description of the FSI between the final pion and the nucleus. Thus, based on the SL amplitudes, we can construct a pion-nucleus optical potential that is consistent with the transition operators for electroweak pion production off a nucleus. To the best of our knowledge, our approach is the first to provide a consistent framework for treating the medium effect on the pion and electroweak pion production on the same footing. This point is worth emphasizing because it is this consistency that enables us to *predict* cross sections for electroweak coherent pion production *with no adjustable parameters*, once we fix certain parameters (see below) relevant to medium effects by fitting to the pion-nucleus scattering data.

Another point to be noted is that our model takes into account the non-local effect for in-medium Δ-propagation. For neutrino-induced coherent pion production, neither the RS-based nor previous microscopic models have included this effect. As pointed out in Ref. [20], the non-local effect could reduce the cross section by a factor of ~ 2 (~ 1.7) for $E_\nu = 0.5$ (1) GeV. We consider it important to take due account of the possibly large non-local effect.

Our calculation adopts the following procedure. We first construct a pion-nucleus optical potential, employing the SL πN scattering (on- and off-shell) amplitudes as basic ingredient. The medium modification of the Δ-propagation in a nucleus is considered with the use of the Δ-hole model [19]. All the free parameters in our model (spreading potential, phenomenological terms in the optical potential) are fixed by fitting to pion-nucleus scattering

data. After these parameters are determined, we are in a position to make prediction on the coherent pion production process. Before calculating the neutrino-induced process, we test the reliability of our model by comparing our predictions for the photo-induced process with data. After finding satisfactory results for the photo-process, we proceed to calculate neutrino-induced coherent pion production.

The organization of this paper is as follows. Sec. II is dedicated to the explanation of our approach. We first introduce the elementary amplitudes of the SL model. We then give expressions for calculating the electroweak coherent pion production amplitudes in terms of the SL amplitudes and derive the cross section formulae. The expression for the constructed optical potential and its relation with the scattering amplitude are also given there. We present numerical results in Sec. III, and give a conclusion in Sec. IV. Appendix A provides the definition of the multipole amplitudes, while Appendix B explains the Lorentz transformation used in our calculation. In Appendix C we give expressions for quantities that appear in the Δ-hole model.

II. FORMULATION

The kinematics of the reactions under consideration is as follows. We consider coherent pion production in neutrino(ν_ℓ)-nucleus(t) scattering: $\nu_\ell(p_\nu)+t(p_t)\to\ell^-(p'_\ell)+\pi^+(k)+t(p'_t)$ for the CC process, and $\nu_\ell(p_\nu)+t(p_t)\to\nu_\ell(p'_\ell)+\pi^0(k)+t(p'_t)$ for the NC process; we also consider the antineutrino-counterparts. The four-momentum for each particle in the laboratory frame (LAB) is given in the parentheses. The four-momentum transfer from the leptons is denoted by $q^\mu\equiv p_\nu^\mu-p_\ell'^\mu$. We choose a right-handed coordinate system in which the z-axis lies along the incident neutrino momentum $\boldsymbol{p}_\nu$, and the y-axis is taken along $\boldsymbol{p}_\nu\times\boldsymbol{p}'_\ell$. In evaluating a nuclear matrix element, it is convenient to work in the pion-nucleus center-of-mass frame (ACM). The kinematical variables in ACM are denoted by $\boldsymbol{q}_A$, $\boldsymbol{k}_A$, etc. We also work in the pion-*nucleon* CM frame (2CM), when calculating the elementary SL amplitudes. The kinematical variables in 2CM are denoted by $\boldsymbol{q}_2$, $\boldsymbol{k}_2$, etc. When working in ACM (2CM), we choose a coordinate system in which the z-axis lies along $\boldsymbol{q}_A$ ($\boldsymbol{q}_2$) and the y-axis is along $\boldsymbol{p}_{\nu,A}\times\boldsymbol{p}'_{\ell,A}$ ($\boldsymbol{p}_{\nu,2}\times\boldsymbol{p}'_{\ell,2}$).

A. The SL Model

We express nuclear transition amplitudes for coherent pion production in terms of the elementary amplitudes derived from the SL model [17]. In this section, therefore, we introduce the SL amplitudes. The differential cross section in the LAB frame for pion production in the neutrino-*nucleon* CC reaction, $\nu_\ell(p_\nu)+N(p_N)\to\ell^-(p'_\ell)+\pi^+(k)+N(p'_N)$, is given by

(cf. Eq. (10) of Ref. [17])

$$\frac{d^5\sigma}{dE'_\ell d\Omega'_\ell d\Omega_\pi} = \frac{G_F^2\cos^2\theta_c}{2}\left(\frac{|\boldsymbol{k}|}{\omega_\pi}+\frac{|\boldsymbol{k}|-\hat{\boldsymbol{k}}\cdot(\boldsymbol{p}_\nu-\boldsymbol{p}'_\ell)}{E'_N}\right)^{-1}\frac{|\boldsymbol{p}'_\ell|}{|\boldsymbol{p}_\nu|}\frac{|\boldsymbol{k}|^2 m_N^2}{\omega_\pi E_N E'_N}\frac{L^{\mu\nu}W_{\mu\nu}}{(2\pi)^5}\ , \tag{1}$$

where $G_F = 1.16637\times10^{-5}$ GeV^{-2} is the Fermi constant, and θ_c is the Cabbibo angle ($\cos\theta_c = 0.974$). E'_ℓ and ω_π are the energies of the final lepton and pion, respectively, m_N is the nucleon mass, and E_N (E'_N) is the initial (final) nucleon energy. $W_{\mu\nu}$ and $L^{\mu\nu}$ represent the hadron and the lepton tensors, respectively, and their definitions are found in Ref. [17] [Eqs. (11), (12)]. The above cross section can be written as

$$\begin{aligned}\frac{d^5\sigma}{dE'_\ell d\Omega'_\ell d\Omega_\pi} &= \frac{G_F^2\cos^2\theta_c}{2}\left(\frac{|\boldsymbol{k}|}{\omega_\pi}+\frac{|\boldsymbol{k}|-\hat{\boldsymbol{k}}\cdot(\boldsymbol{p}_\nu-\boldsymbol{p}'_\ell)}{E'_N}\right)^{-1}\frac{|\boldsymbol{p}'_\ell||\boldsymbol{k}|^2}{(2\pi)^5|\boldsymbol{p}_\nu|}E'_{\ell,2}p_{\nu,2} \\ &\times\ \frac{1}{2}\sum_{s_N s'_N}\sum_{s'_\ell}|\Gamma_{2L}(F^V-F^A)|^2\ ,\end{aligned} \tag{2}$$

where F^V and F^A are the transition amplitudes in which the hadronic vector and the axial-vector currents are respectively contracted with the leptonic current. The symbol s_N (s'_N) is the z-component of the initial (final) nucleon spin, while s'_ℓ denotes the final lepton spin. The energies of the final lepton and the initial neutrino in 2CM are denoted by $E'_{\ell,2}$ and $p_{\nu,2}$, respectively. F^V and F^A, including both hadronic and lepton currents, are calculated in 2CM, and then embedded in the cross section expression given in LAB. The factor Γ_{2L} arises from the relevant Lorentz transformation (see Appendix B):

$$\Gamma_{2L} = \sqrt{\frac{\omega_{\pi,2}E_{N,2}E'_{N,2}}{\omega_\pi E_N E'_N}}\ , \tag{3}$$

where $\omega_{\pi,2}$, $E_{N,2}$ and $E'_{N,2}$ are the energies of the pion, the incident nucleon and the final nucleon in 2CM. The spin structure of F^V and F^A can be parametrized as

$$\begin{aligned}F^V = &-i\vec{\sigma}\cdot\vec{\epsilon}_\perp F_1^V - \vec{\sigma}\cdot\hat{k}_2\vec{\sigma}\cdot\hat{q}_2\times\vec{\epsilon}_\perp F_2^V - i\vec{\sigma}\cdot\hat{q}_2\hat{k}_2\cdot\vec{\epsilon}_\perp F_3^V - i\vec{\sigma}\cdot\hat{k}_2\hat{k}_2\cdot\vec{\epsilon}_\perp F_4^V \\ &-i\vec{\sigma}\cdot\hat{q}_2\hat{q}_2\cdot\vec{\epsilon}F_5^V - i\vec{\sigma}\cdot\hat{k}_2\hat{q}_2\cdot\vec{\epsilon}F_6^V + i\vec{\sigma}\cdot\hat{k}_2\epsilon_0 F_7^V + i\vec{\sigma}\cdot\hat{q}_2\epsilon_0 F_8^V\ ,\end{aligned} \tag{4}$$

where $\vec{\epsilon}_\perp = \hat{q}_2\times(\vec{\epsilon}\times\hat{q}_2)$ and

$$\begin{aligned}F^A = &-i\vec{\sigma}\cdot\hat{k}_2\vec{\sigma}\cdot\vec{\epsilon}_\perp F_1^A - \vec{\sigma}\cdot\hat{q}_2\times\vec{\epsilon}_\perp F_2^A - i\vec{\sigma}\cdot\hat{k}_2\vec{\sigma}\cdot\hat{q}_2\hat{k}_2\cdot\vec{\epsilon}_\perp F_3^A - i\hat{k}_2\cdot\vec{\epsilon}_\perp F_4^A \\ &-i\vec{\sigma}\cdot\hat{k}_2\vec{\sigma}\cdot\hat{q}_2\hat{q}_2\cdot\vec{\epsilon}F_5^A - i\hat{q}_2\cdot\vec{\epsilon}F_6^A + i\epsilon_0 F_7^A + i\vec{\sigma}\cdot\hat{k}_2\vec{\sigma}\cdot\hat{q}_2\epsilon_0 F_8^A\,.\end{aligned} \tag{5}$$

The lepton-current matrix element ϵ^μ is given by $\epsilon^\mu = \langle\ell|\bar{\psi}_l\gamma^\mu(1-\gamma_5)\psi_\nu|\nu_\ell\rangle$. We have introduced parametrization for F^A simply via $F^A = \vec{\sigma}\cdot\hat{k}_2F^V$. The amplitudes, F_i^V and F_i^A, are expressed in terms of the multipole amplitudes $E_{l\pm}^{V,A}, M_{l\pm}^{V,A}, S_{l\pm}^{V,A}$ and $L_{l\pm}^A$, which are functions of q^2 and W (the πN invariant mass) and computed in 2CM. Their explicit expressions are presented in Appendix A.

In a coherent process on a spin-zero target under consideration, only the spin non-flip terms of the transition amplitudes contribute. We therefore can work with $\bar{F}^{V(A)}$ defined by

$$\bar{F}^{V(A)} = \frac{1}{2}\mathrm{Tr}[F^{V(A)}] \ , \tag{6}$$

where the trace is taken for nucleon spin space. Their explicit forms are

$$\bar{F}^{V} = -\hat{k}_2 \cdot \hat{q}_2 \times \vec{\epsilon}_\perp F_2^V \ , \tag{7}$$

and

$$\begin{aligned} \bar{F}^{A} \ = \ & -i\hat{k}_2 \cdot \vec{\epsilon}_\perp F_1^A - i\hat{k}_2 \cdot \hat{q}_2 \hat{k}_2 \cdot \vec{\epsilon}_\perp F_3^A - i\hat{k}_2 \cdot \vec{\epsilon}_\perp F_4^A \\ & -i\hat{k}_2 \cdot \hat{q}_2 \hat{q}_2 \cdot \vec{\epsilon} F_5^A - i\hat{q}_2 \cdot \vec{\epsilon} F_6^A + i\epsilon_0 F_7^A + i\hat{k}_2 \cdot \hat{q}_2 \epsilon_0 F_8^A \ . \end{aligned} \tag{8}$$

In particular, the resonant parts of the elementary amplitudes are given by

$$\begin{aligned} \bar{F}_R^V - \bar{F}_R^A \ = \ & \Big(-2\hat{k}_2 \cdot \hat{q}_2 \times \vec{\epsilon}_\perp M_{R\ 1+}^{(3/2),V} - 2i\hat{k}_2 \cdot \vec{\epsilon}_\perp E_{R\ 1+}^{(3/2),A} \\ & -4i\hat{k}_2 \cdot \hat{q}_2 \epsilon_0 S_{R\ 1+}^{(3/2),A} + 4i\hat{k}_2 \cdot \hat{q}_2 \hat{q}_2 \cdot \vec{\epsilon} L_{R\ 1+}^{(3/2),A} \Big) \Lambda_{ij}^{3/2} \ , \end{aligned} \tag{9}$$

where the suffix "R" stands for the resonant parts of the corresponding multipole amplitudes associated with the excitation of the Δ resonance. From the resonant amplitude we can factor out the Δ-propagator, $D(W)$, as

$$\bar{F}_R^V - \bar{F}_R^A = \frac{N(k_2, q_2)}{D(W)} \ , \tag{10}$$

and

$$D(W) = W - m_\Delta - \Sigma_\Delta(W) \ , \tag{11}$$

where m_Δ and Σ_Δ are the bare mass and self energy of the Δ-resonance, respectively.

We next discuss the T-matrix element for πN scattering, which serves as an input for constructing an optical potential for pion-nucleus scattering. A calculational procedure for the πN T-matrix within the SL model can be found in Ref. [16]. A distorted wave obtained with this optical potential will be used to take account of the final-state interaction in coherent pion production. The T-matrix is decomposed into the resonant (t_R) and non-resonant (t_{nr}) parts as

$$t_{\pi N}^{(c)} = t_R^{(c)} + t_{nr}^{(c)} \ , \tag{12}$$

where the superfix c specifies a channel; in our model the resonance amplitude exists only for the P_{33} channel. The on-shell component of the T-matrix given in Eq. (12) is related to the phase shift by

$$t_{\pi N}^{(c)} = -\frac{W}{\pi \omega_{\pi,2} E_{N,2}} \frac{e^{2i\delta^{(c)}} - 1}{2ik_2^o} \ , \tag{13}$$

where W is the invariant mass of the πN system, and $\omega_{\pi,2} = \sqrt{k_2^{o\,2} + m_\pi^2}$ and $E_{N,2} = \sqrt{k_2^{o\,2} + m_N^2}$ are the on-shell energies of the pion and the nucleon in 2CM, respectively. The resonant amplitude is expressed as

$$t_R^{(P_{33})}(k_2', k_2; W) = -\frac{F_{\pi N\Delta}(k_2') F_{\pi N\Delta}(k_2)}{D(W)} \ , \tag{14}$$

where $F_{\pi N\Delta}(k_2)$ is the dressed $\pi N\Delta$ vertex, and $D(W)$ is the Δ propagator introduced in Eq. (11). We note that the four-momenta, k_2 and k_2', are in general off-energy-shell.

B. Coherent pion production in neutrino-nucleus scattering

Similarly to Eq. (12) for the πN scattering amplitude, the weak amplitudes $\bar{F}^{V(A)}$, defined in Eqs. (6)–(8), also have a resonant $\bar{F}_R^{V(A)}$ and non-resonant $\bar{F}_{nr}^{V(A)}$ parts. Accordingly, the transition amplitudes of coherent pion production on nuclei have the resonant and non-resonant parts. We now describe how these two components are calculated in our approach.

1. transition matrix element: resonant part

The main task in calculating the resonant part of coherent pion production on nuclei is to account for the medium effects on Δ propagation in the elementary resonant amplitudes $F_R^{V(A)}$. Here we follow the procedure of the Δ-hole model of pion-nucleus reactions by modifying the Δ propagator in Eq. (11). Thus it is useful to first briefly explain how the Δ-hole model is formulated by considering the elastic pion-nucleus scattering; for a full account of the formulation see Refs. [21, 22, 23, 24].

The Δ-hole model is formulated within the projection operator formalism[21]. The nuclear Fock space is divided into four spaces; P_0, P_1, D and Q. The P_0-space is spanned by the pion and the nuclear ground state, the P_1-space by the pion and one-particle one-hole states, the D-space by the one-Δ one-hole configurations, and $Q = 1 - P_0 - P_1 - D$ contains the reminder of the full space. A projected Hamiltonian is written as, e.g., $H_{P_0D} = P_0 H D$. Starting with the Schrödinger equation in the full space ($H|\Psi\rangle = E|\Psi\rangle$), we can apply the standard projection operator techniques[21] to obtain an equation, defined only in the P_0-space, to describe the pion-nucleus elastic scattering T-matrix. In the Δ-hole model, one further imposes the condition that the D-space is the doorway of the transitions between $P = P_0 + P_1$ and Q spaces; namely $H_{PQ} = H_{QP} = 0$. The pion-nucleus scattering amplitude due to the Δ excitation can then be written as

$$T_{P_0P_0}(E) = H_{P_0D} G_{\Delta h}(E) H_{DP_0} \ , \tag{15}$$

where the total energy defined in ACM ($E + Am_N$) is given by

$$E + Am_N = q_A^0 + \sqrt{\boldsymbol{q}_A^2 + (Am_N)^2} = \sqrt{\boldsymbol{k}_A^2 + m_\pi^2} + \sqrt{\boldsymbol{k}_A^2 + (Am_N)^2} \ , \tag{16}$$

where A is the mass number. The Δ-hole propagator $G_{\Delta h}$ in Eq. (15) is defined by

$$G_{\Delta h}^{-1} = D(E - H_\Delta) - W_{el} - \Sigma_{\rm pauli} - \Sigma_{\rm spr} \ . \tag{17}$$

Here $D(E - H_\Delta)$ can be calculated from Eq. (11) with H_Δ being the Hamiltonian for the Δ-particle in the nuclear many-body system. The effects due to the Q-space are included in the so-called spreading potential, $\Sigma_{\rm spr}$. A microscopic calculation of the spreading potential is very complicated since it involves the calculation of pion absorption by two or more nucleons. It is therefore a common practice to determine $\Sigma_{\rm spr}$ phenomenologically by fitting to the pion-nucleus scattering data. Excitations to the P_1-space are included in the Δ self energy $\Sigma_\Delta(W)$ of $D(E - H_\Delta)$ [see Eq. (11)] with a correction due to the Pauli blocking ($\Sigma_{\rm pauli}$). De-excitation to the P_0-space is the rescattering in the elastic mode, and is denoted by W_{el}. In our actual calculation, we expand $G_{\Delta h}$ in term of W_{el}, and the expansion series is resummed by solving the Lippmann-Schwinger equation.

The calculations of the pion-nucleus scattering amplitude in Eq. (15) require a diagonalization of the Δ-hole propagator $G_{\Delta h}$ of Eq. (17). For the diagonalization, it is practically convenient to work with the oscillator basis for the Δ state, defined by the Hamiltonian H_Δ, and the nucleon hole state. This diagonalization is a difficult numerical task. Although an efficient method using the doorway state expansion has been developed [23], the diagonalization of $G_{\Delta h}$ is still difficult, particularly for heavier nuclei. In Ref. [19], Karaoglu and Moniz (KM) proposed a simplified calculation with the Δ-hole model in which $G_{\Delta h}$ is calculated with a local density approximation rather than a diagonalization. In their simplified treatment, $\Sigma_{\rm pauli}$ is calculated by a nuclear matter calculation[25], and their result is given in Appendix C. Their parametrization of the spreading potential $\Sigma_{\rm spr}$ in terms of a central and a spin-orbit terms are also given in Appendix C. Each term of the spreading potential has a complex strength, which are determined by fitting to the pion-nucleus scattering data. KM applied their approach to π-^{16}O scattering, and found a good agreement between their calculation with data, and also with the full Δ-hole calculation [22, 23] except for the most central partial waves. Encouraged by this success, we follow this simplified version of the Δ-hole model to include the medium effects on the Δ propagation in defining the electroweak pion production matrix elements.

Schematically, the resonant part of the transition matrix element, $\mathcal{M}_R^A$, of weak coherent pion production on nuclei induced by the charged current can be obtained by replacing the initial H_{DP_0} of Eq. (15) by $H_{DP_0'}$ where P_0' is the space spanned by the (axial-)vector current and the nucleus in the ground state. In terms of the single particle wave functions $\psi_j(\boldsymbol{p}_N)$

of the nucleons in the initial and final nuclear states, we thus have[2]

$$\begin{aligned}\mathcal{M}_R^A &= \sum_j \int \frac{d^3p_N}{(2\pi)^3}\frac{d^3p'_N}{(2\pi)^3}\psi_j^*(\boldsymbol{p}'_N)\frac{\Gamma_{2A}N(k_2,q_2)(2\pi)^3\delta(\boldsymbol{p}_N+\boldsymbol{q}_A-\boldsymbol{p}'_N-\boldsymbol{k}_A)}{D(E+m_N-H_\Delta)-\Sigma_{\rm pauli}-\Sigma_{\rm spr}}\psi_j(\boldsymbol{p}_N) \\ &= \sum_j \int \frac{d^3p_\Delta}{(2\pi)^3}\psi_j^*(\boldsymbol{p}'_N)\frac{\Gamma_{2A}N(k_2,q_2)}{D(E+m_N-H_\Delta)-\Sigma_{\rm pauli}-\Sigma_{\rm spr}}\psi_j(\boldsymbol{p}_N)\ , \end{aligned} \tag{18}$$

where $\boldsymbol{p}_\Delta = \boldsymbol{p}_N + \boldsymbol{q}_A = \boldsymbol{p}'_N + \boldsymbol{k}_A$; the index j denotes single particle quantum numbers including the isospin . The summation ($\sum_j$) is taken over the occupied states of the nucleus. The factor Γ_{2A} is defined by

$$\Gamma_{2A} = \sqrt{\frac{\omega_{\pi,2}E_{N,2}E'_{N,2}}{\omega_{\pi,A}E_{N,A}E'_{N,A}}}\ , \tag{19}$$

where ω_π, E_N and E'_N are the energies of the pion, the incoming nucleon and the outgoing nucleon, respectively, and the quantities in the numerator (denominator) refer to 2CM (ACM). This factor arises from the fact that $\bar{F}_R^{V(A)}$ computed in 2CM are to be embedded in $\mathcal{M}_R^A$ evaluated in ACM. To evaluate the numerator in the integrand of Eq. (18), we clearly need a prescription for relating variables in 2CM to those in ACM. Here we use the commonly used prescription [27, 28] to fix the nucleon momenta with the lepton momentum transfer $\boldsymbol{q}_A$ and outgoing pion momentum $\boldsymbol{k}_A$ as

$$\boldsymbol{p}_N = -\frac{\boldsymbol{q}_A}{A} - \frac{A-1}{2A}(\boldsymbol{q}_A-\boldsymbol{k}_A)\ , \qquad \boldsymbol{p}'_N = -\frac{\boldsymbol{k}_A}{A} + \frac{A-1}{2A}(\boldsymbol{q}_A-\boldsymbol{k}_A)\ , \tag{20}$$

and write the πN invariant mass as

$$W = \sqrt{(E_{N\,A}+q_A^0)^2-(\boldsymbol{p}_N+\boldsymbol{q}_A)^2}\ , \tag{21}$$

with $E_{N\,A} = \sqrt{\boldsymbol{p}_N^2+m_N^2}$. Having specified all the relevant variables in ACM, we can derive the corresponding variables in 2CM via a Lorentz transformation to obtain $N(k_2,q_2)$ of Eq. (18). For more details about this Lorentz transformation (including the discussion of a somewhat different treatment of an off-shell pion momentum), see Appendix B. Note that, in treating the wave functions, $\psi(\boldsymbol{p}_N)$ and $\psi(\boldsymbol{p}'_N)$, and the Δ kinetic term in the denominator in the integrand of Eq. (18), we do *not* use the prescription given in Eqs. (20) and (21); thus the important recoil effects on Δ-propagation are not neglected in our calculations.

We incorporate the recoil effect on the Δ self-energy in the first order approximation. This is done by linearizing the Δ-propagator with the following expansion[24]:

$$D(E+m_N-H_\Delta)\ \sim\ D(W)-\gamma(W)(H_\Delta-e_\Delta^0), \tag{22}$$

[2] In Ref. [26], the authors carried out a calculation for photon-induced coherent pion production by diagonalizing $G_{\Delta h}$.

$$E + m_N = W + e^0_\Delta \ , \tag{23}$$

$$\gamma(W) = \partial D(W)/\partial W, \tag{24}$$

$$H_\Delta = \frac{\boldsymbol{p}^2_\Delta}{2\mu_\Delta} + V_\Delta + V^C_\Delta + e_N, \tag{25}$$

$$1/\mu_\Delta = 1/m_\Delta + 1/(A-1)m_N \ , \tag{26}$$

where V_Δ (V^C_Δ) is the Δ (Coulomb) potential in the nucleus, and e_N is the hole energy. The Δ potential is taken to be the same as that for the nucleon; its explicit expression is given in Appendix C. Equation (23) defines e^0_Δ. To carry out the integration over the Δ momentum $\boldsymbol{p}_\Delta$ in Eq. (18), we express the nucleon wave function $\psi_j(\boldsymbol{p})$ in terms of its coordinate-space form $\phi_j(\boldsymbol{r})$. We note that with the prescription in Eqs. (20) and (21), the numerator $N(k_2, q_2)$ of Eq. (18) is independent of the variable $\boldsymbol{p}_\Delta$ and can be factorized out of the integration. With this factorization approximation and with the use of the linearized form in Eq. (22), the integration over $\boldsymbol{p}_\Delta$ leads to the following r-space expression:

$$\mathcal{M}^A_R = -\left(\frac{\mu_\Delta \Gamma_{2A} N(k_2, q_2)}{2\pi\gamma}\right) \sum_j \int d^3r d^3r' \phi^*_j(\boldsymbol{r}') e^{-i\boldsymbol{k}_A\cdot\boldsymbol{r}'} \frac{e^{iK_\Delta|\boldsymbol{r}'-\boldsymbol{r}|}}{|\boldsymbol{r}'-\boldsymbol{r}|} e^{i\boldsymbol{q}_A\cdot\boldsymbol{r}} \phi_j(\boldsymbol{r}) \ , \tag{27}$$

where

$$K^2_\Delta = \frac{2\mu_\Delta}{\gamma}\left\{W - m_\Delta - \Sigma_\Delta(W) + \gamma(E - W + m_N) - \gamma\left[e_N + V_\Delta + V^C_\Delta\right] - \Sigma_{\rm pauli} - \Sigma_{\rm spr}\right\} \tag{28}$$

Following the procedure described in Ref. [19] [see Eqs. (25)–(39) therein], and subsequently applying the Lorentz transformation from ACM to LAB, we obtain the following expression for the transition matrix element $\mathcal{M}^L_R$ in LAB

$$\begin{aligned}
\mathcal{M}^L_R = {} & \frac{16\sqrt{1+|\lambda|}\pi}{3} \frac{\mu_\Delta D(W)}{\gamma} \Gamma_{2L} \\
\times {} & \left(-2\hat{k}_2\cdot\hat{q}_2\times\vec{\epsilon}_\perp M^{(3/2),V}_{R\ 1+} - 2i\hat{k}_2\cdot\vec{\epsilon}_\perp E^{(3/2),A}_{R\ 1+} - 4i\hat{k}_2\cdot\hat{q}_2\epsilon_0 S^{(3/2),A}_{R\ 1+} + 4i\hat{k}_2\cdot\hat{q}_2\hat{q}_2\cdot\vec{\epsilon} L^{(3/2),A}_{R\ 1+}\right) \\
\times {} & \sum_{N=p,n}(1+\frac{\lambda\tau_N}{2}) \int s^2 ds R^2 dR j_0(pR) j_0(Ps) \frac{e^{i\bar{K}_\Delta s}}{s} \left\{1 + \frac{i\mu_\Delta s}{\bar{K}_\Delta}\left[\bar{e_N} + H_N\right]\right\} \rho_N(R) \hat{j}_1(k_F s) \ ,
\end{aligned} \tag{29}$$

where $p = |\boldsymbol{k}_A - \boldsymbol{q}_A|$, $P = |\boldsymbol{k}_A + \boldsymbol{q}_A|/2$, $s = |\boldsymbol{r}' - \boldsymbol{r}|$, $R = |\boldsymbol{r}' + \boldsymbol{r}|/2$, and $\bar{K}_\Delta$ is obtained from K_Δ by replacing e_N with its average value, $\bar{e}_N$; we choose $\bar{e}_N = 16$ MeV. The 2CM variables k_2 and q_2 are obtained from k_A and q_A using the Lorentz transformation as mentioned above. The variable λ denotes the charge state of the outgoing pion, while $\tau_N = 1\,(-1)$ for $N =$ proton (neutron). The factor Γ_{2L} is from the Lorentz transformation from 2CM to LAB and is defined by

$$\Gamma_{2L} = \sqrt{\frac{\omega_{\pi,2} E_{N,2} E'_{N,2}}{\omega_{\pi,L} E_{N,L} E'_{N,L}}} \ . \tag{30}$$

In Eq. (29), $j_\ell(x)$ is the spherical Bessel function of order ℓ, and $\hat{j}_1(x) \equiv \frac{3}{x} j_1(x)$; k_F is the Fermi momentum

$$k_F^3(R) = \frac{3\pi^2}{2}\rho_N(R) \ . \tag{31}$$

The proton (neutron) matter density is denoted by ρ_p (ρ_n), and is normalized to the total number of protons (neutrons) inside the target. For the proton matter form factor we use the empirical nuclear charge form factor [29] divided by the proton charge form factor [30]. The neutron matter density is assumed to be the same as the proton matter density.

The single nucleon Hamiltonian appearing in Eq. (29) is given by

$$H_N = -\frac{\nabla_s^2}{2m_N} - \frac{\nabla_R^2}{8m_N} + V\left[(R^2 + s^2/4)^{1/2}\right] \ , \tag{32}$$

where V is the single particle potential [Eq. (C8)].

To take account of the final pion-nucleus interactions, we convolute the matrix element $\mathcal{M}_R^L$ of Eq. (29) with the pion distorted wave which is expanded in partial waves:

$$\chi_\lambda^*(\boldsymbol{k}'_A) = \sum_{l_\pi m_\pi} \chi^*_{\lambda\, l_\pi}(k'_A) Y^*_{l_\pi m_\pi}(\hat{\boldsymbol{k}}_A) Y_{l_\pi m_\pi}(\hat{\boldsymbol{k}}'_A) \ , \tag{33}$$

where k'_A is the off-shell momentum. We note that the pion distorted wave also depends on the pion charge (λ). More details on our calculations of the pion wave functions are given in Sec. II D.

By performing the partial wave decomposition of $\mathcal{M}_R^L$ (now defined by the off-shell pion momentum by setting $\boldsymbol{k}_A \to \boldsymbol{k}'_A$) and using Eq. (33), the amplitude $\mathcal{M}_R^L$ with pion-nucleus FSI takes the following form:

$$\begin{aligned} \mathcal{M}_R^L \ = \ & \epsilon_A^\mu \sum_{l_\pi} \Big[P^1_{l_\pi}(x_A) \left(\cos\phi_A^\pi I^{l_\pi\, 1}_{E\,\mu} - i \sin\phi_A^\pi I^{l_\pi\, 1}_{M\,\mu} \right) \\ & + P^1_{l_\pi}(x_A) \left(\sin\phi_A^\pi I^{l_\pi\, 2}_{E\,\mu} + i\cos\phi_A^\pi I^{l_\pi\, 2}_{M\,\mu} \right) - 2P_{l_\pi}(x_A) I^{l_\pi\, 3}_{L\,\mu} + 2P_{l_\pi}(x_A) I^{l_\pi\, 0}_{S\,\mu} \Big] \ , \end{aligned} \tag{34}$$

where $x_A = \hat{q}_A \cdot \hat{k}_A$, ϕ_A^π is the azimuthal angle of the pion, and ϵ_A^μ is the lepton current matrix element in ACM. The associated Legendre function of degree l_π and order 0 (1) is denoted by P_{l_π} ($P^1_{l_\pi}$). We have introduced the quantities $I^{l_\pi\,\nu}_{X\,\mu}$ defined by

$$\begin{aligned} I^{l_\pi\,\nu}_{X\,\mu} = & -i\frac{32\sqrt{1+|\lambda|}\pi\mu_\Delta}{3} \int dk'_A k'^2_A \ \chi^*_{\lambda\, l_\pi}(k'_A) \ \int dx'_A \Lambda^\nu_\mu \Gamma^\chi_{AL} \Gamma_{2AL} \gamma^{-1} X_R \xi^X_{1 l_\pi}(x'_A) \\ & \times \sum_{N=p,n} (1 + \frac{\lambda\tau_N}{2}) \int s^2 ds R^2 dR j_0(pR) j_0(Ps) \frac{e^{i\bar{K}_\Delta s}}{s} \left\{ 1 + \frac{i\mu_\Delta s}{\bar{K}_\Delta} \left[e^-_N + H_N \right] \right\} \rho_N(R) \hat{j}_1(k_F s) \ , \end{aligned} \tag{35}$$

where $x'_A = \hat{q}_A \cdot \hat{k}'_A$, $x'_2 = \hat{q}_2 \cdot \hat{k}'_2$, and

$$\xi^X_{\ell l_\pi}(x'_A) \ = \ \begin{cases} \dfrac{2l_\pi + 1}{2l_\pi(l_\pi+1)} P^1_\ell(x'_2) P^1_{l_\pi}(x'_A) \ , & (X = E, M) \\ \dfrac{2l_\pi + 1}{2} P_\ell(x'_2) P_{l_\pi}(x'_A) \ , & (X = L, S) \end{cases} \tag{36}$$

and

$$\frac{X_R}{D(W)} = E_{R\ 1+}^{(3/2),A}\ ,\ M_{R\ 1+}^{(3/2),V}\ ,\ L_{R\ 1+}^{(3/2),A}\ ,\ S_{R\ 1+}^{(3/2),A}\ , \tag{37}$$

for $X = E, M, L, S$.

The Lorentz transformation factors coming from the electroweak amplitudes (Γ_{2AL}) and the wave function (Γ^χ) in Eq. (34) are respectively

$$\Gamma_{2AL} = \sqrt{\frac{\omega'_{\pi,2}E'_{N,2}E^i_{N,2}}{\omega'_{\pi,A}E'_{N,L}E^i_{N,L}}}\ , \qquad \Gamma^\chi = \sqrt{\frac{\omega_{\pi,A}E''_{N,A}E^f_{N,A}}{\omega_{\pi,L}E''_{N,L}E^f_{N,L}}}\ , \tag{38}$$

where ω'_π is the pion energy in the intermediate state, E^i_N and E^f_N are the nucleon energies in the initial and final states while E'_N and E''_N are those in the intermediate states; in general, E'_N and E''_N can be different. As before, the suffices $\{2, A, L\}$ attached to the energies specify reference frames. It is noted that the multipole amplitudes (X^A_R) depend on x'_A because the πN invariant mass in the intermediate state depends on it [Eqs. (20) and (21)]. We also have introduced the Lorentz matrix Λ^ν_μ defined by $\epsilon^\nu_2 = \Lambda^\nu_\mu \epsilon^\mu_A$; Λ^ν_μ also depends on x'_A; the same Lorentz matrix relates q_A (k'_A) to q_2 (k'_2). A procedure for deriving the Lorentz matrix and the transformation factors in Eq. (38) are explained in Appendix B.

2. transition matrix element: non-resonant part

We assume that there is no medium effect on the non-resonant part, $\bar{F}^V_{nr} - \bar{F}^A_{nr}$, of the weak pion production amplitude on a nucleon in nuclei. Including the final pion-nucleus interactions and using the same factorization approximation based on the choice Eq. (20) of the nucleon momenta to evaluate $\bar{F}^V_{nr} - \bar{F}^A_{nr}$, the non-resonant coherent pion production matrix element $\mathcal{M}^L_{nr}$ can be written as

$$\mathcal{M}^L_{nr} = \sum_{N=p,n} \int d^3k'_A \chi^*_\lambda(\boldsymbol{k}'_A)\Gamma^\chi_{AL}\Gamma_{2AL}F_N(\boldsymbol{k}'_A - \boldsymbol{q}_A)(\bar{F}^{V,\zeta}_{nr} - \bar{F}^{A,\zeta}_{nr})\ , \tag{39}$$

where $\bar{F}^{V,\zeta}_{nr}$ ($\bar{F}^{A,\zeta}_{nr}$) is the non-resonant part of $\bar{F}^V$ ($\bar{F}^A$) given in Eqs. (7) and (8). $\bar{F}^{V(A)}_{nr}$ depends on N and λ [Eq. (A17)], and the set (N, λ) is collectively denoted by ζ. The nuclear form factor $F_N(\boldsymbol{p})$ is given by

$$F_N(\boldsymbol{p}) = \int d^3r \rho_N(\boldsymbol{r}) e^{i\boldsymbol{p}\cdot\boldsymbol{r}}\ . \tag{40}$$

After the partial wave expansion of the pion distorted wave, we arrive at

$$\begin{aligned}\mathcal{M}^L_{nr} \ =\ & \epsilon^\mu_A \sum_{l_\pi} \Big[P^1_{l_\pi}(x_A)\left(\cos\phi^\pi_A J^{l_\pi\,1}_{E\,\mu} - i\sin\phi^\pi_A J^{l_\pi\,1}_{M\,\mu}\right) \\ & + P^1_{l_\pi}(x_A)\left(\sin\phi^\pi_A J^{l_\pi\,2}_{E\,\mu} + i\cos\phi^\pi_A J^{l_\pi\,2}_{M\,\mu}\right) - P_{l_\pi}(x_A) J^{l_\pi\,3}_{L\,\mu} + P_{l_\pi}(x_A) J^{l_\pi\,0}_{S\,\mu}\Big]\ ,\end{aligned} \tag{41}$$

where we have introduced $J^{l_\pi\,\nu}_{X\,\mu}$ defined by

$$J^{l_\pi\,\nu}_{X\,\mu} = -4\pi i \int dk'_A k'^2_A \; \chi^*_{\lambda\, l_\pi}(k'_A) \int dx'_A \Lambda^\nu_\mu \Gamma^X_{AL} \Gamma_{2AL} \times \sum_\ell \xi^X_{\ell l_\pi}(x'_A) \sum_{N=p,n} X^{\ell,\zeta}_{nr} \int r^2 dr \rho_N(r) j_0(pr) \; , \tag{42}$$

for $X = E, M, L, S$. The multipole amplitudes are included in $X^{\ell,\zeta}_{nr}$ as

$$X^{\ell,\zeta}_{nr} = (\ell+1)^2 X^{A,\zeta}_{nr\,\ell+} + \ell^2 X^{A,\zeta}_{nr\,\ell-} \; , \tag{43}$$

for $X = L, S$, and

$$E^{\ell,\zeta}_{nr} = (\ell+1) E^{A,\zeta}_{nr\,\ell+} - \ell E^{A,\zeta}_{nr\,\ell-} \; , \tag{44}$$

$$M^{\ell,\zeta}_{nr} = (\ell+1) M^{V,\zeta}_{nr\,\ell+} + \ell M^{V,\zeta}_{nr\,\ell-} \; , \tag{45}$$

for $X = E, M$. The ζ dependence of the multipole amplitudes is indicated explicitly. For example, $E^{A,\zeta}_{nr\,\ell+}$ is the non-resonant part of $E^A_{\ell+}$ which has been introduced previously. The same rule applies to the other multipole amplitudes.

3. Cross Section

Having written the transition amplitude for the coherent process in terms of the SL multipole amplitudes, we can proceed to calculate the cross section for the CC process. First, we write the transition amplitudes in Eqs. (34) and (41) as

$$\mathcal{M}^L_R = \bar{\mathcal{M}}^L_{R,\mu} \epsilon^\mu_A$$
$$\mathcal{M}^L_{nr} = \bar{\mathcal{M}}^L_{nr,\mu} \epsilon^\mu_A \; .$$

In the Laboratory frame, the differential cross sections for $\nu_\ell(p_\nu) + t(p_t) \to \ell^-(p'_\ell) + \pi^+(k) + t(p'_t)$ is then given by

$$\frac{d^5\sigma}{dE'_\ell d\Omega'_\ell d\Omega_\pi} = \frac{G_F^2 \cos^2\theta_c}{2} \left(\frac{|\boldsymbol{k}|}{\omega_\pi} + \frac{|\boldsymbol{k}| - \hat{\boldsymbol{k}} \cdot (\boldsymbol{p}_\nu - \boldsymbol{p}'_\ell)}{E'_t} \right)^{-1} \frac{|\boldsymbol{p}'_\ell||\boldsymbol{k}|^2}{(2\pi)^5 |\boldsymbol{p}_\nu|} E'_{\ell,A} p_{\nu,A} \times \sum_{s'_\ell} |(\bar{\mathcal{M}}^L_{R,\mu} + \bar{\mathcal{M}}^L_{nr,\mu}) \epsilon^\mu_A|^2 \; , \tag{46}$$

where $E'_t \left(= \sqrt{\boldsymbol{p}'^2_t + (Am_N)^2} \right)$ is the total energy of the nucleus in the final state in LAB, and $E'_{\ell,A}$ and $p_{\nu,A}$ are the energies of the final lepton and the initial neutrino in ACM. Note that the calculation of $\sum_{s'_\ell} |(\bar{\mathcal{M}}^L_{R,\mu} + \bar{\mathcal{M}}^L_{nr,\mu}) \epsilon^\mu_A|^2$ of Eq. (46) can make use of the following property:

$$L^{\mu\nu}_A \equiv \frac{E'_{\ell,A} p_{\nu,A}}{2} \sum_{s'_\ell} \epsilon^\mu_A \epsilon^{\nu *}_A = p^\mu_{\nu,A} p'^\nu_{\ell,A} + p^\nu_{\nu,A} p'^\mu_{\ell,A} - g^{\mu\nu} p_{\nu,A} \cdot p'_{\ell,A} \pm i \epsilon^{\mu\nu\rho\sigma} p_{\nu,A\,\rho} p'_{\ell,A\,\sigma} \; , \tag{47}$$

where $g^{\mu\nu}$ is the geometric tensor and $\epsilon^{\mu\nu\rho\sigma}$ is the antisymmetric tensor with $\epsilon^{0123} = 1$. The plus (minus) sign in the last term is for the (anti-)neutrino process.

To obtain the cross section formula for the neutrino NC process, $\nu + t \to \nu + \pi^0 + t$, we make the following changes in Eq.(46): Remove the Cabbibo angle. Set the lepton mass equal to zero. Set the pion charge index λ (and ζ) to zero in $I^{l_\pi\,\nu}_{X\,\mu}$ and $J^{l_\pi\,\nu}_{X\,\mu}$ ($X = E, M, L, S$) in Eqs. (35) and (42). (Note that the pion wave function ($\chi_{\lambda\, l_\pi}$) also contains λ-dependence.) Finally, multiply the multipole amplitudes $M^{(3/2,1/2),V}_{\ell+}$ with $(1 - 2\sin^2\theta_W)$, where θ_W is the Weinberg angle ($\sin^2\theta_W = 0.23$), and multiply $M^{(0),V}_{\ell+}$ with $(-2\sin^2\theta_W)$.

For the anti-neutrino CC process, the result for the neutrino CC process is modified as follows. Set the pion charge index λ (and ζ) to -1 in $I^{l_\pi\,\nu}_{X\,\mu}$ and $J^{l_\pi\,\nu}_{X\,\mu}$. Replace the lepton current by the one for the anti-neutrino process, which amounts to adopting the negative sign in the leptonic tensor, Eq. (47). What modifications are needed for getting the cross section for the anti-neutrino NC process is now obvious.

C. Coherent Pion Photo-Production

With the same derivation given above, we can also get an expression for the differential cross section of the coherent π^0 photo-production process $\gamma(q) + t(p_t) \to \pi^0(k) + t(p'_t)$ in the LAB frame:

$$\frac{d^2\sigma}{d\Omega_\pi} = \frac{\alpha}{2\pi}\left(\frac{|\boldsymbol{k}|}{\omega_\pi} + \frac{|\boldsymbol{k}| - \hat{k}\cdot\boldsymbol{q}}{E'_t}\right)^{-1} \frac{|\boldsymbol{k}|^2}{|\boldsymbol{q}|\omega_\pi}\frac{1}{2}\sum_\epsilon |\mathcal{M}^\gamma_R + \mathcal{M}^\gamma_{nr}|^2 \,, \tag{48}$$

where α is the fine structure constant, and $\frac{1}{2}\sum_\epsilon$ stands for averaging over the photon polarization. The transition amplitudes $\mathcal{M}^\gamma_R$ and $\mathcal{M}^\gamma_{nr}$ for the photo-process are obtained from Eqs. (34) and (41) by retaining only the vector current, setting $\phi^\pi_A = 0$, and regarding ϵ^μ_A as the polarization vector of the incident photon. Finally, the pion charge index (λ) is set to zero in $I^{l_\pi\,\nu}_{X\,\mu}$ and $J^{l_\pi\,\nu}_{X\,\mu}$ [Eqs. (35) and (42)].

D. Optical Potential for Pion-Nucleus Scattering

We calculate the pion-nucleus scattering using the computer code, PIPIT [31] by appropriately modifying the optical potential there to accommodate the dynamical features of the Δ-hole model and the SL model. In the original PIPIT, the optical potential (U), which is derived within the multiple scattering formalism by Kerman, McManus and Thaler

(KMT) [32], is given by[3]

$$U(\boldsymbol{k}'_A, \boldsymbol{k}_A) = \frac{A-1}{A} \left\{ \rho_p(\boldsymbol{q}) t_{\pi p}(\boldsymbol{k}'_A, \boldsymbol{k}_A; k^o_A) + \rho_n(\boldsymbol{q}) t_{\pi n}(\boldsymbol{k}'_A, \boldsymbol{k}_A; k^o_A) \right\} \ , \tag{49}$$

where $\boldsymbol{k}_A$ ($\boldsymbol{k}'_A$) is the incoming (outgoing) pion momentum in ACM, and k^o_A the magnitude of the on-shell momentum. The quantities $\rho_p(\boldsymbol{q})$ ($\rho_n(\boldsymbol{q})$) is the form factor of the proton (neutron) matter distribution for $\boldsymbol{q} = \boldsymbol{k}_A - \boldsymbol{k}'_A$, and $t_{\pi p}$ ($t_{\pi n}$) is the pion-proton (pion-neutron) scattering T-matrix whose normalization has been defined in Eq. (13). It is to be noted that this original optical potential does not take account of Δ-propagation in nuclei. In Ref. [19], KM separated $t_{\pi p}$ ($t_{\pi n}$) into the resonant and non-resonant parts, took the non-resonant and the Coulomb parts of the optical potential from the PIPIT code, and combined it with the resonant part derived from a simplified Δ-hole model. A phenomenological s-wave potential which is proportional to the square of the nuclear density ($\rho_t = \rho_p + \rho_n$) was also included to account for the pion absorption by two nucleons through non-Δ mechanisms. Thus the KM optical potential is given by

$$U(\boldsymbol{k}'_A, \boldsymbol{k}_A) = U_{nr} + U_R + U_{ph}(\rho_t^2) \ , \tag{50}$$

where U_{nr}, U_R and U_{ph} are the non-resonant, resonant and phenomenological parts, respectively.

In constructing our optical potential, we follow the same separation as in Eq. (50). The non-resonant part of the optical potential is obtained from the PIPIT code by replacing the non-resonant T-matrices in the original code with those derived from the SL model. It is worth emphasizing that the SL model provides both on-shell and off-shell T-matrix elements. Another difference from the original PIPIT code is that we use a different prescription for the Lorentz transformation from ACM to 2CM, as explained in Appendix B.

Regarding the resonant part, we use the resonant part of πN T-matrix from the SL model, basically following the procedure used in Ref. [19] (apart from a more elaborate treatment of kinematics (Lorentz transformation, etc.)). First, we expand the optical potential into partial waves as

$$U(\boldsymbol{k}'_A, \boldsymbol{k}_A) = \frac{2}{\pi} \sum_{l_\pi m_\pi} V^{l_\pi}(k'_A, k_A) Y^*_{l_\pi m_\pi}(\hat{k}'_A) Y_{l_\pi m_\pi}(\hat{k}_A) \ . \tag{51}$$

The resonant part of the potential is (cf. Eq. (39) of Ref. [19])

$$V^{l_\pi}_R(k'_A, k_A) = \frac{A-1}{A} \frac{8\pi^2 \mu_\Delta}{3} \int dx_A \Gamma_{A2} \gamma^{-1} x_2 P_{l_\pi}(x_A) F_{\pi N\Delta}(k'_2) F_{\pi N\Delta}(k_2) \tag{52}$$

$$\times \sum_{N=p,n} (1 + \frac{\lambda \tau_N}{2}) \int s^2 ds R^2 dR j_0(pR) j_0(Ps) \frac{e^{i\bar{K}_\Delta s}}{s} \left\{ 1 + \frac{i\mu_\Delta s}{\bar{K}_\Delta} [e^-_N + H_N] \right\} \rho_N(R) \hat{j}_1(k_F s) \ ,$$

[3] PIPIT also includes a finite-range Coulomb interaction, and corrections from the truncated part of the Coulomb interaction are taken into account using the Vincent-Phatak method [33].

where $\boldsymbol{k}_2$ ($\boldsymbol{k}'_2$) is the incoming (outgoing) pion momentum in 2CM, and $x_A = \hat{k}_A \cdot \hat{k}'_A$, $x_2 = \hat{k}_2 \cdot \hat{k}'_2$, $P = |\boldsymbol{k}_A + \boldsymbol{k}'_A|/2$, $p = |\boldsymbol{k}_A - \boldsymbol{k}'_A|$. The dressed $\pi N\Delta$ coupling ($F_{\pi N\Delta}$) has been introduced in Eq. (14). The Lorentz transformation of the T-matrix from 2CM to ACM gives rise to the factor Γ_{A2} defined by

$$\Gamma_{A2} = \sqrt{\frac{\omega_{\pi,2}\,\omega'_{\pi,2}\,E_{N,2}E'_{N,2}}{\omega_{\pi,A}\,\omega'_{\pi,A}\,E_{N,A}E'_{N,A}}}\ , \tag{53}$$

with $\omega^{(\prime)}_{\pi,2} = \sqrt{\boldsymbol{k}^{(\prime)\,2}_2 + m^2_\pi}$, $\omega^{(\prime)}_{\pi,A} = \sqrt{\boldsymbol{k}^{(\prime)\,2}_A + m^2_\pi}$, $E^{(\prime)}_{N,2} = \sqrt{\boldsymbol{k}^{(\prime)\,2}_2 + m^2_N}$ and $E^{(\prime)}_{N,A} = \sqrt{\boldsymbol{p}^{(\prime)\,2}_{N,A} + m^2_N}$. The values of $\boldsymbol{k}^{(\prime)}_2$ and $\boldsymbol{p}^{(\prime)}_{N,A}$ are fixed according to the prescription explained in Appendix B. The other quantities have already been introduced in Sec. II B 1.

Finally, we discuss the phenomenological term, U_{ph}. We assume that in coordinate space U_{ph} can be parametrized as

$$U_{ph}(\boldsymbol{r}) = B\left(\frac{\rho_t(r)}{\rho_t(0)}\right)^2\ , \tag{54}$$

where B is the partial wave dependent strength of the potential. The corresponding partial wave potential in momentum space is given by

$$V^{l_\pi}_{ph}(k'_A, k_A) = \frac{A-1}{A}4\pi^3 B_{l_\pi}\int_{-1}^{1} dx_A P_{l_\pi}(x_A)\int dr r^2 j_0(pr)\left(\frac{\rho_t(r)}{\rho_t(0)}\right)^2\ . \tag{55}$$

In the present calculation we include V^0_{ph} and V^1_{ph} and treat their strengths B_0 and B_1 as adjustable parameters. Thus our model contains as free parameters B_0 and B_1 (complex numbers) in addition to the couplings in the spreading potential.

Given the optical potential, we solve the Lippmann-Schwinger equation

$$T'_{l_\pi}(k'_A, k_A; k^o_A) = V_{l_\pi}(k'_A, k_A; k^o_A) + \frac{2}{\pi}\int \frac{V_{l_\pi}(k'_A, \bar{k}_A; k^o_A)T'_{l_\pi}(\bar{k}_A, k_A; k^o_A)\bar{k}^2_A d\bar{k}_A}{\omega_\pi(k^o_A) + E_t(k^o_A) - \omega_\pi(\bar{k}_A) - E_t(\bar{k}_A) + i\epsilon}\ . \tag{56}$$

The solution to this equation will be used in two contexts. First, we use it to calculate pion-nucleus elastic and total scattering cross sections, and compare them with data to find the optimal values of the free parameters in our model. The solution to Eq. (56) is also used to compute the pion distorted wave function that features in the matrix elements in Eqs. (35) and (42). For the former purpose, we obtain the full T-matrix of pion-nucleus scattering from T' in Eq. (56) using the relation

$$T = \frac{A}{A-1}T'\ . \tag{57}$$

For charged-pion scattering, corrections for the finite range Coulomb potential are incorporated with the use of the Vincent-Phatak method [33]. The procedure for calculating

scattering observables from T is detailed in Ref. [31]. For the latter purpose, we calculate the pion distorted wave $\chi^*_{l_\pi}(k_A)$ associated with T' using the relation

$$\chi^*_{l_\pi}(k_A) = \frac{\delta(k_A - k^o_A)}{k^2_A} + \frac{T'_{l_\pi}(k^o_A, k_A; k^o_A)}{\omega_\pi(k^o_A) + E_t(k^o_A) - \omega_\pi(k_A) - E_t(k_A) + i\epsilon} \ , \tag{58}$$

where, for notational simplicity, dependence on the pion charge (λ) is suppressed. Following the KMT formalism [32], we use $\chi^*_{l_\pi}(k_A)$ in evaluating the matrix elements in Eqs. (35) and (42). This wave function is related to the full wave function by

$$\chi^{(\mathrm{full})*}_{l_\pi} = -\frac{1}{A-1} + \frac{A}{A-1}\chi^*_{l_\pi} \ . \tag{59}$$

For charged-pion scattering, $\chi^{(\mathrm{full})*}_{l_\pi}$ does not have the correct normalization, because the Coulomb potential has been cut off at a finite distance; this entails the necessity of multiplying $\chi^{(\mathrm{full})*}_{l_\pi}$ with a normalization factor (call it κ). We note that it is $\chi^*_{l_\pi}$ rather than $\chi^{(\mathrm{full})*}_{l_\pi}$ that enters into our calculation, and we choose to use the same normalization factor κ for $\chi^*_{l_\pi}$ as for $\chi^{(\mathrm{full})*}_{l_\pi}$. Thus, in evaluating the matrix elements in Eqs. (35) and (42), we use $\kappa\chi^*_{l_\pi}$ instead of $\chi^*_{l_\pi}$. In the Δ resonance region of our interest, it turns out that $|\kappa - 1| \lesssim 0.01$. (For neutral pion scattering, $\kappa = 1$.)

III. NUMERICAL RESULTS

A. Pion-Nucleus Scattering

As explained in the previous sections, our model contains four complex free parameters. Two of them are the central (V_C) and LS (V_{LS}) parts of the spreading potential [see Eq. (C5)], and the other two are the strengths, B_0 and B_1, of the s-wave and p-wave phenomenological terms in the optical potential [see Eq. (55)]. These free parameters are optimized to fit the pion-nucleus scattering data. Since our aim here is to calculate coherent pion production off ^{12}C, we should use the $\pi - ^{12}$C scattering data to fix these parameters. Adjusting them to reproduce the total cross sections and the elastic differential cross sections for $\pi - ^{12}$C scattering, we obtain:

$$\begin{aligned} V_C &= 48.0 - 34.5i \text{ MeV} \ , \qquad V_{LS} = -3.0 - 2.0i \text{ MeV} \\ B_0 &= 5.1 + 5.2i \text{ MeV} \ , \qquad B_1 = 2.8 - 5.7i \text{ MeV} \ . \end{aligned} \tag{60}$$

We note that our calculations include the pion-nucleus partial waves up to $l_\pi \leq 9$ [Eq. (56)], and s- and p-waves (and all possible spin-isospin states) for the elementary πN scattering.[4]

[4] Hereafter, we include the same set of partial waves (l_π) in the amplitudes for both pion-nucleus scattering and pion production off a nucleus. For the non-resonant elementary pion production amplitudes, we include the partial waves up to $\ell \leq 4$ in Eq. (42).

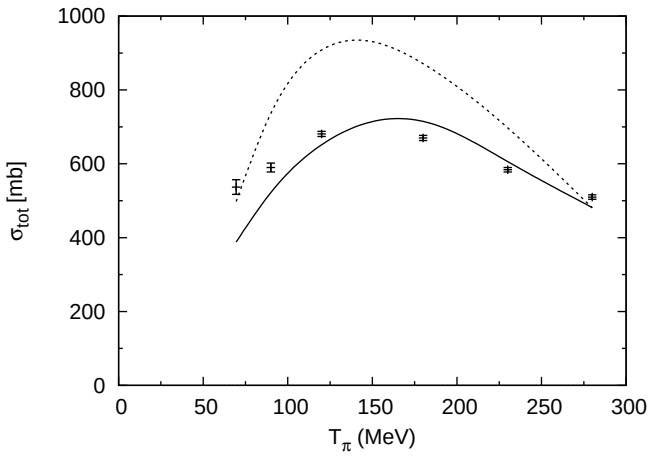

FIG. 1: Total cross sections for $\pi^- - {}^{12}$C scattering. The solid curve is obtained with our full calculation, while the dashed curve is obtained without the spreading potential. The data are from Ref. [34].

Figures. 1 and 2 illustrate the quality of fit to the $\pi - {}^{12}$C scattering data achieved in our model (with our optical potential). In Fig. 1, the total cross sections for π^--^{12}C scattering are shown as a function of the pion kinetic energy T_π in the laboratory frame. The results of our full calculation are given by the solid curve and, for comparison, the results obtained without the spreading potential are also shown in the dashed curve. We observe a large reduction in the total cross section as we go from the dashed to solid lines, which is mainly caused by the strong pion absorption simulated by the spreading potential. In connection with fitting to the pion-nucleus scattering data, it is worthwhile to make the following comment. In the calculation of coherent pion production, the final-state interaction is nothing but elastic scattering between the pion and nucleus. One might therefore think that a phenomenological adjustment of the pion-nucleus optical potential to fit the elastic pion-nucleus scattering data will be good enough. However, in our consistent model building, the spreading potential enters not only into the optical potential but also into the pion production operators, and hence it is important to control its strength using the total cross section data. The fact that the spreading potential has a very large effect on the total cross sections makes this point particularly important.

Our results for the differential cross sections are shown in Fig. 2. In addition to our full calculation shown in the solid curve, we also show in the dashed curve the results obtained without the phenomenological term U_{ph} [see Eq. (54)]. We see that this phenomenological ρ^2 term, which simulates absorption of s-wave and p-wave pions by two-nucleons within our model, is not large in the considered $T_\pi > 40$ MeV region for $\pi-{}^{12}$C elastic scattering. However it is known that U_{ph} can play an important role for many observables in low-energy

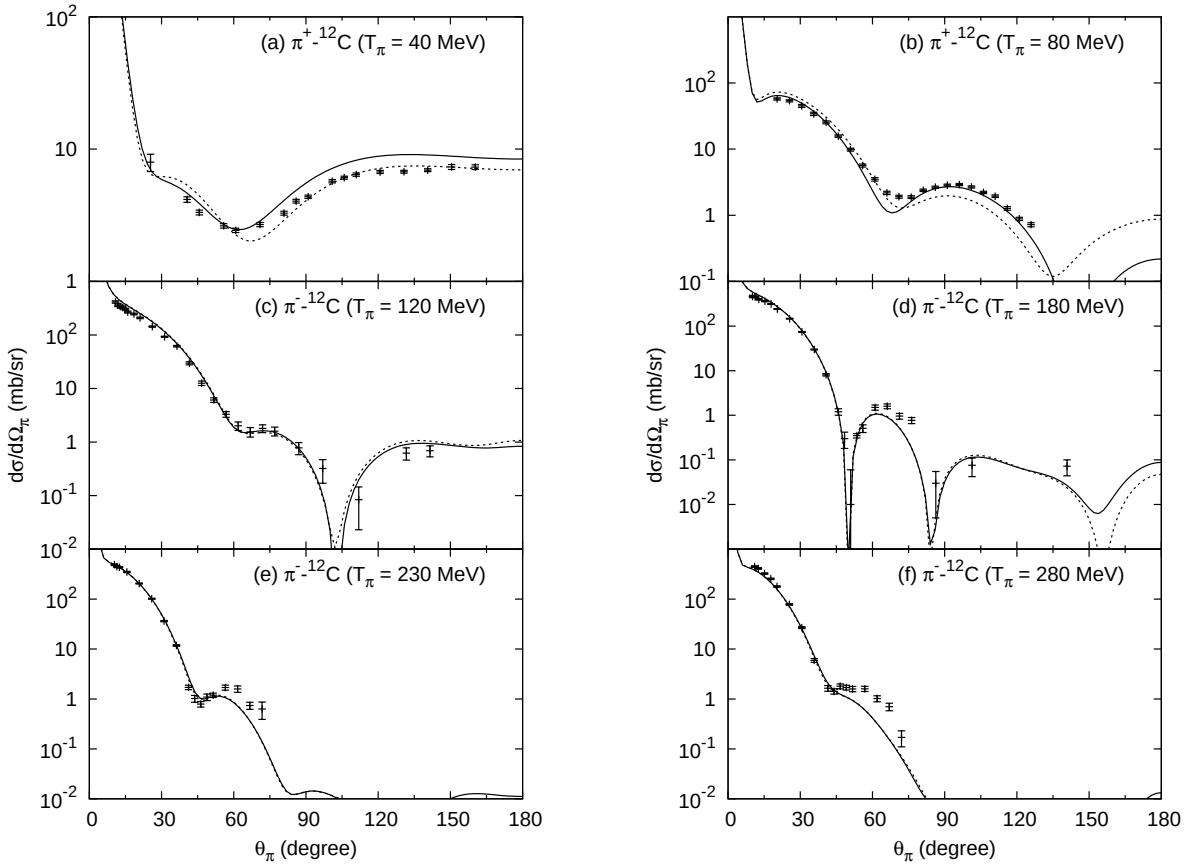

FIG. 2: $\pi-^{12}$C elastic differential cross sections. The solid curve is obtained with our full calculation while the dashed curve is obtained without the phenomenological terms in Eq. (54). The data are from Ref. [35] for (a), Ref. [36] for (b) and Ref. [34] for (c)-(f).

pion-nucleus scattering. As an example to shed light on this point, we have calculated $\pi - {}^{16}O$ elastic scattering at $T_\pi = 50$ MeV using the same model (only the nuclear density is different). We have found that, in reproducing the data satisfactorily in our approach, the ρ^2 term plays an important role, its size being almost as large as that found in Fig. 4(a) of Ref. [19]. Overall, the results of our full calculation satisfactorily reproduce the data for both the total and elastic cross sections.

B. Coherent Pion Photo-Production

We are now in a position to perform a parameter-free calculation of the cross sections for coherent pion production. The photo-process, for which extensive data are available, provides a good testing ground for checking the reliability of our approach. We compare in Fig. 3 our numerical results for the differential cross sections for $\gamma + {}^{12}\mathrm{C}_{g.s.} \to \pi^0 + {}^{12}\mathrm{C}_{g.s.}$ with the existing data [37, 38]. The long-dash lines are obtained without FSI and without the

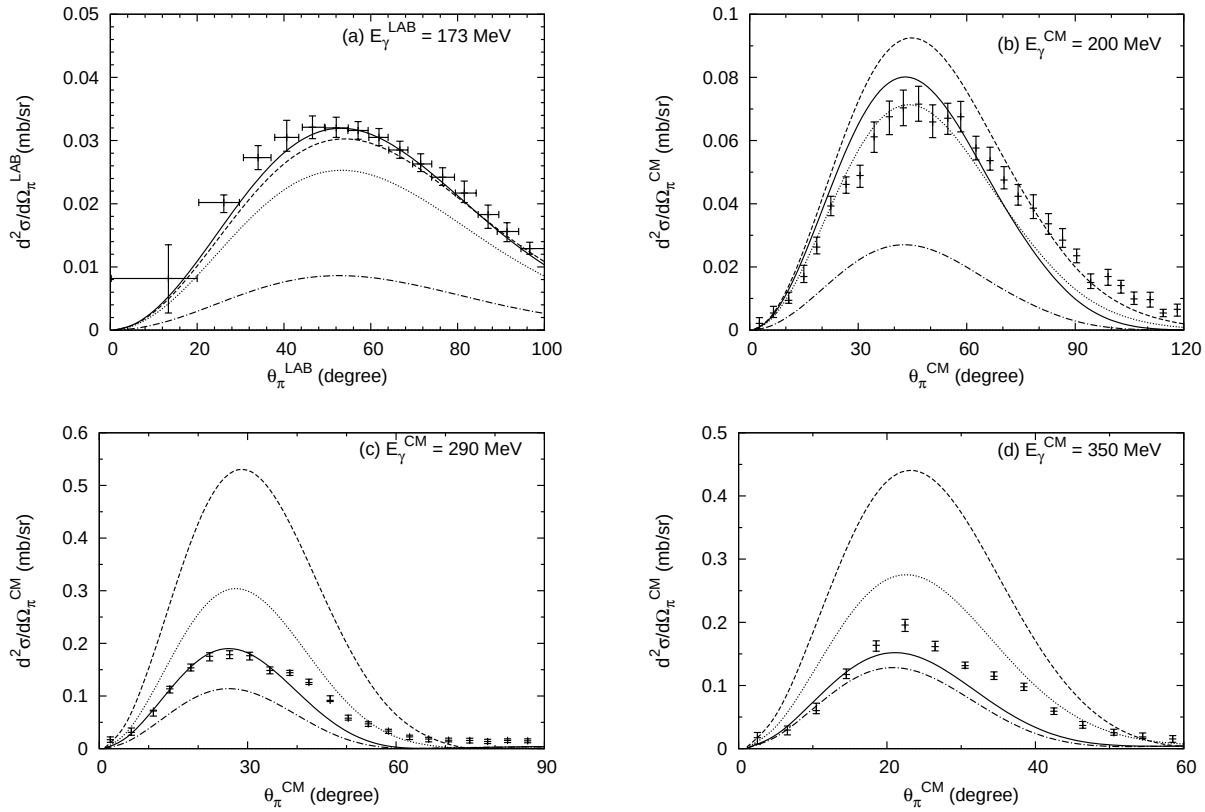

FIG. 3: Differential cross sections for $\gamma + {}^{12}\mathrm{C}_{g.s.} \to \pi^0 + {}^{12}\mathrm{C}_{g.s.}$ for different incident photon energies (indicated in each panel). The solid lines represent the results of the full calculation. The dashed lines are obtained without the FSI and without the medium effects on the Δ-propagation, while the dotted lines are obtained with the medium effects on the Δ included. The dash-dotted curves correspond to a case in which the pion production operator includes only the Δ mechanism. For more detailed explanations for the different cases, see the text. The data are from Ref. [37] for (a) and from Ref. [38] for (b)-(d).

medium effects on Δ-propagation.[5] With the medium effects on the Δ included, the short-dash lines are obtained, and the results of our full calculation are given by the solid lines. Figure 3 indicates that the medium effects are quite sizable, and they play an important role in bringing the calculated differential cross sections in agreement with the data. Particularly noteworthy is the drastic reduction of the cross section in the Δ region [Fig. 3 (c)], a feature that reflects the fact that a significant part of the medium effects simulate pion absorption. The good general agreement seen in Fig. 3 indicates the basic soundness of the method we

[5] The "medium effects on the Δ" here refer to the combined effects of the Pauli blocking of Δ-decay ($\Sigma_{\rm pauli}$), the spreading potential ($\Sigma_{\rm spr}$), and the terms in the square bracket in Eq. (28).

have used in determining the spreading potential.

It is true that, for higher incident energies, in the large angle region beyond the peak position, there are noticeable discrepancies between the results of our full calculation and the data. However, as noted in Ref. [38], the data in this region are likely to be substantially contaminated by incoherent processes in which the final nucleus is in its low-lying excited states. The effects of this type of contamination are expected to grow for higher incident photon energies and for larger momentum transfers (the large angle region) because of increased nuclear excitations. We therefore take the viewpoint that the discrepancy found in Figs. 3 (b)-(d) does not necessarily signal a failure of our model, and that our model describes coherent pion photo-production reasonably well.

Figure 3 also shows (in the dash-dotted lines) the results corresponding to a case in which the pion production operator includes only the Δ mechanism (the non-resonant mechanism turned off); [6] the distorted pion wave function incorporating FSI is the same as that used for the full calculation. These results serve to demonstrate the importance of the non-resonant mechanism. Fig. 3 (a) indicates that, near threshold, the contributions from the resonant and non-resonant mechanisms are comparable, a feature that is not surprising away from the resonance peak. A remarkable feature is that even near the resonance energy [see Fig. 3 (c)] the contribution from the non-resonant mechanism is quite significant. This is partly because the resonant contribution is considerably suppressed by pion absorption (the spreading potential) and the non-local effect of Δ propagation (the Δ kinetic term).[7]

To summarize this section, the results for the coherent photo-pion production process establish to a satisfactory degree the reliability of our present approach (*i.e.,* combined use of the SL model and the Δ-hole model) and motivate us to apply the same approach to neutrino-induced coherent pion production.

C. Neutrino-Induced Coherent Pion Production

We now present the numerical results of our calculations for neutrino-induced coherent pion production on the ^{12}C target. We consider the CC and NC processes induced by a neutrino or an anti-neutrino:

$$\begin{aligned} \nu_\mu + {}^{12}\mathrm{C}_{g.s.} &\rightarrow \mu^- + \pi^+ + {}^{12}\mathrm{C}_{g.s.} \\ \nu + {}^{12}\mathrm{C}_{g.s.} &\rightarrow \nu + \pi^0 + {}^{12}\mathrm{C}_{g.s.} \end{aligned} \tag{61}$$

[6] In the SL model, the resonant amplitude itself contains the non-resonant mechanism. We refer to the purely non-resonant amplitudes as "non-resonant amplitudes", and it is only these non-resonant amplitudes that we turn off here and later in Figs. 5-8 and 10.

[7] We come back to the non-local effect due to the Δ kinetic term later when we discuss the neutrino-induced processes.

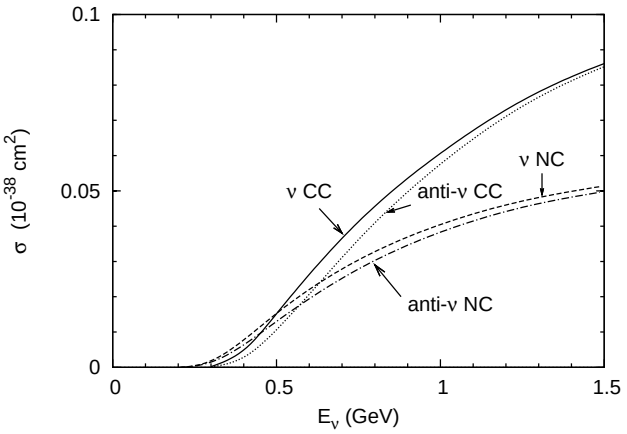

FIG. 4: The E_ν-dependence of the total cross section for $\nu_\mu + {}^{12}\mathrm{C}_{g.s.} \to \mu^- + \pi^+ + {}^{12}\mathrm{C}_{g.s.}$ (solid line), $\nu + {}^{12}\mathrm{C}_{g.s.} \to \nu + \pi^0 + {}^{12}\mathrm{C}_{g.s.}$ (dashed line), $\bar{\nu}_\mu + {}^{12}\mathrm{C}_{g.s.} \to \mu^+ + \pi^- + {}^{12}\mathrm{C}_{g.s.}$ (dotted line) and $\bar{\nu} + {}^{12}\mathrm{C}_{g.s.} \to \bar{\nu} + \pi^0 + {}^{12}\mathrm{C}_{g.s.}$ (dash-dotted line).

$$\bar{\nu}_\mu + {}^{12}\mathrm{C}_{g.s.} \ \to \ \mu^+ + \pi^- + {}^{12}\mathrm{C}_{g.s.}$$
$$\bar{\nu} + {}^{12}\mathrm{C}_{g.s.} \ \to \ \bar{\nu} + \pi^0 + {}^{12}\mathrm{C}_{g.s.}$$

Figure 4 gives the total cross sections for these processes as functions of the incident neutrino (anti-neutrino) energy in the laboratory system, E_ν. It is seen that, for higher incident energies, the ratio σ_{CC}/σ_{NC} approaches 2, a value expected from the isospin factor. For lower incident energies ($E_\nu \lesssim 500$ MeV), however, σ_{NC} is larger than σ_{CC}, reflecting the fact that the phase space for the CC process is reduced significantly by the muon mass. It is well known that interference between the vector and axial-vector currents can lead to different cross sections for the neutrino and anti-neutrino processes. However, since the coherent process is dominated by the contribution of the axial current (see Fig. 9), the role of the interference term is diminished drastically. This explains why in Fig. 4 the cross sections for the neutrino and anti-neutrino processes are almost the same.

To compare our results with data, we need to evaluate the total cross sections averaged over the neutrino fluxes that pertain to the relevant experiments. We choose to use the fluxes up to $E_\nu \leq 2$ GeV and neglect the fluxes beyond that limit based on the following consideration. Since our model includes no resonances other than the Δ, it is expected to be reliable only for $W \lesssim 1.4$ GeV. The fact that even at $E_\nu = 1$ GeV coherent pion production can involve contributions coming from the $W > 1.4$ GeV region is disquieting, but we can still expect that the Δ-excitation contribution is predominant for the total cross section for the coherent process. [This feature can be seen in, *e.g.*, Fig. 5 to be discussed later.] For $E_\nu \sim 2$ GeV, we do expect that Δ dominance gets significantly less pronounced but that Δ still gives the most important contribution. Meanwhile, the region $E_\nu \gtrsim 1.5$ GeV belongs

to the tail of the neutrino flux used in MiniBooNE. We therefore consider it reasonable to compare with data our theoretical cross section averaged over the neutrino flux up to $E_\nu = 2$ GeV. For the CC process, we use the flux reported in Ref. [39] and deduce

$$\sigma_{\rm ave}^{CC} = 6.3 \times 10^{-40}{\rm cm}^2 \ . \tag{62}$$

A K2K experiment [1] reports the upper limit

$$\sigma_{\rm K2K} < 7.7 \times 10^{-40}{\rm cm}^2 \ . \tag{63}$$

In fact, this upper limit corresponds to events satisfying the muon momentum cut, $p_\mu > 450$ MeV and the cut on the momentum transfer squared, $Q^2_{\rm rec} < 0.1$ GeV^2; $Q^2_{\rm rec}$ is calculated as

$$Q^2_{\rm rec} = 2E_\nu^{\rm rec}(E_\mu - p_\mu \cos\theta_\mu) - m_\mu^2 \ , \tag{64}$$

where the reconstructed neutrino energy ($E_\nu^{\rm rec}$) is calculated from the muon kinematics [the energy (E_μ) and the scattering angle (θ_μ)] assuming the quasi-elastic kinematics:

$$E_\nu^{\rm rec} = \frac{1}{2}\frac{(m_p^2 - m_\mu^2) - (m_n - V)^2 + 2E_\mu(m_n - V)}{(m_n - V) - E_\mu + p_\mu \cos\theta_\mu} \ , \tag{65}$$

where m_p, m_n and m_μ are the masses of the proton, neutron and muon, respectively and the nuclear potential (V) is set to 27 MeV. Our result in Eq.(62) is also obtained with these cuts, and is consistent with the K2K data. We note that a recent report from SciBooNE [2] gives a similar empirical upper limit.

For the NC process, we use the flux reported by MiniBooNE in Ref. [40] and arrive at

$$\sigma_{\rm ave}^{NC} = 2.8 \times 10^{-40}{\rm cm}^2 \ . \tag{66}$$

This is to be compared with

$$\sigma_{\rm MiniBooNE} = 7.7 \pm 1.6 \pm 3.6 \times 10^{-40}{\rm cm}^2 \ , \tag{67}$$

given in Ref. [41]. Our result is consistent with the empirical value within the large experimental errors, even though the theoretical value is rather visibly smaller than the empirical central value. It is to be noted however that Ref. [41] is a preliminary report, and that, as discussed in great detail in Ref. [7], $\sigma_{\rm MiniBooNE}$ may be overestimated due to the use of the RS model[6] in the analysis.

We now proceed to present our results for differential observables. In view of the fact that the event rates (cross section times flux) in the K2K, MiniBooNE and SciBooNE experiments [3, 39] have been reported to have a peak around $E_\nu \sim 1$ GeV, we shall often use this energy as a representative in the following presentation. Meanwhile, since the neutrino flux in the planned T2K experiment is expected to have a peak around $E_\nu = 0.6 \sim 0.7$ GeV[42], we shall also present results for lower neutrino energies when that seems useful.

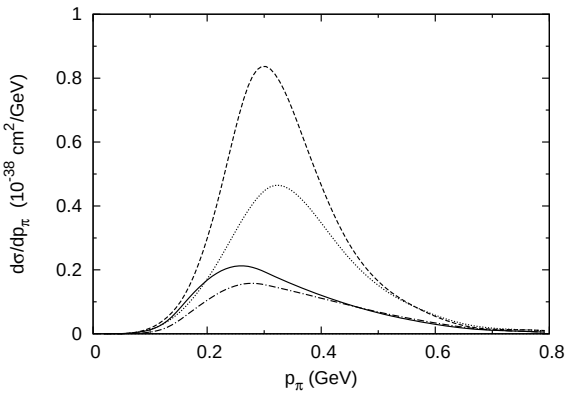

FIG. 5: The pion momentum distribution for $\nu_\mu + {}^{12}\mathrm{C}_{g.s.} \rightarrow \mu^- + \pi^+ + {}^{12}\mathrm{C}_{g.s.}$ at $E_\nu = 1$ GeV; p_π is the pion momentum in the laboratory frame. The use of the solid, dashed, dotted and dash-dotted lines follows the same convention as in Fig. 3.

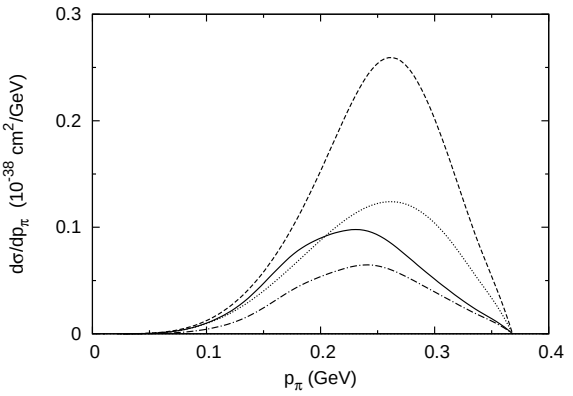

FIG. 6: Same as in Fig. 5 but for $E_\nu = 0.5$ GeV.

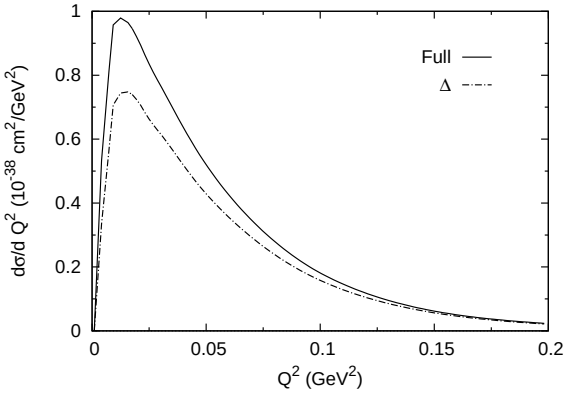

FIG. 7: The Q^2-spectrum for $\nu_\mu + {}^{12}\mathrm{C}_{g.s.} \rightarrow \mu^- + \pi^+ + {}^{12}\mathrm{C}_{g.s.}$ at $E_\nu = 1$ GeV.

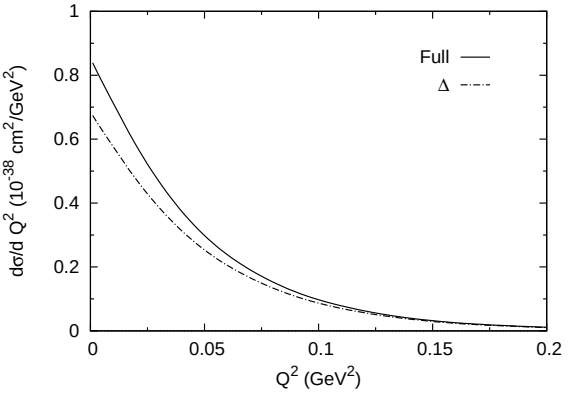

FIG. 8: Same as in Fig. 7 but for the NC process at $E_\nu = 1$ GeV.

The pion momentum spectrum for CC neutrino-induced coherent pion production is shown in Fig. 5 (Fig. 6) for $E_\nu = 1$ GeV (0.5 GeV). The importance of the medium effects manifests itself here in the same manner as in the photo-process (Fig. 3). In the Δ region, strong pion absorption is seen to reduce the cross sections significantly, and FSI shifts the peak position. The dash-dotted line corresponds to a case in which the pion production operator contains only the Δ mechanism (without non-resonant contributions), while the pion optical potential is kept unchanged. We note that, at $E_\nu = 1$ GeV (0.5 GeV), the dash-dotted line corresponds to 82% (64%) of the solid line (the results of the full calculation).

We have seen in the photo-process that the non-resonant mechanism is more important for a smaller energy transfer. To what extent the neutrino case should share this feature is not obvious because the axial-vector current contributions dominate here (see Fig. 9). However, we can see in Figs. 5 and 6 that, in the neutrino case as well, the differential cross sections with smaller pion momenta are more enhanced by the non-resonant mechanism, and that this feature is more prominent for a smaller value of E_ν. A similar tendency is seen for the NC process also. These results indicate that the non-resonant amplitudes in our model, which are dressed by the rescattering, play a significant role in coherent pion production; their role is particularly important for $E_\nu \lesssim 0.5$ GeV. This characteristic feature of our model should be contrasted with the fact that (tree-level) non-resonant mechanisms play essentially no role in any of the previous microscopic calculations for neutrino-induced coherent pion production. A more detailed comparison of the elementary amplitudes used in our present calculation and the previous microscopic-model calculations will be given later in Sec. III E.

We show in Fig. 7 (Fig. 8) the Q^2-distribution for the CC (NC) process. Note that Q^2 defined by $Q^2 \equiv -q^2 \equiv -(p_\nu - p'_\ell)^2$ is different from $Q^2_{\rm rec}$ defined in Eq. (64). Because of the nuclear form factor effect, the distribution rises sharply as Q^2 approaches 0; for the CC process, however, Q^2-distribution becomes zero at $Q^2 = 0$ due to the finite muon mass. Here again we show the results corresponding to a case in which the pion production operator contains only the Δ effect (with non-resonant contributions turned off). The non-resonant mechanism is seen to change the spectrum shape significantly and lead to a sharper peak.

It is informative to examine the individual contributions of the vector and axial-vector currents. We show in Fig. 9 these individual contributions to the neutrino CC process. We find strong dominance of the axial-vector current. The nuclear form factor causes the drastic suppression of non-forward pion production. This aspect combined with the fact that the transverse photon coupling of the vector current [Eq. (7)] forbids forward pion production leads to strong suppression of the vector current contribution. By contrast, since the vertex structure of the axial-vector current favors forward pion production, the strong suppression mechanism at work for the vector current does not apply here. This is the reason why the axial-vector current dominates. This result may be used to argue that incoherent pion production processes in which a nucleus does not break up but transits to excited states, are much less important than coherent pion production in the neutrino-nucleus scattering. As seen in Fig. 3, the incoherent processes give considerable contributions to the total pion production in the photo-process,[8] a feature that may lead to the expectation that the incoherent processes are considerable in the neutrino process as well. However, the

[8] The contributions from the incoherent processes are larger than they appear in Fig. 3 because $\sin\theta_\pi$ needs to be multiplied in integrating over θ_π.

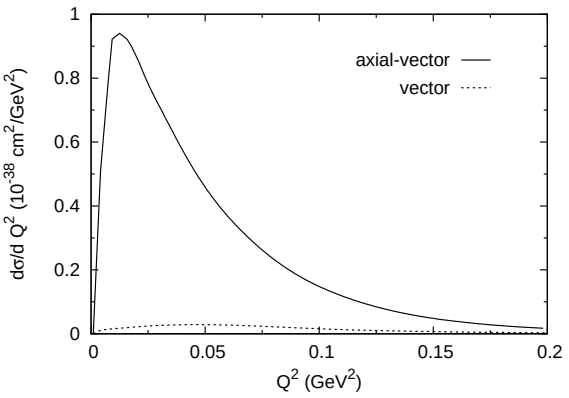

FIG. 9: Contributions from the axial-vector (solid) and vector (dashed) currents for $\nu_\mu + {}^{12}\mathrm{C}_{g.s.} \to \mu^- + \pi^+ + {}^{12}\mathrm{C}_{g.s.}$ at $E_\nu = 1$ GeV.

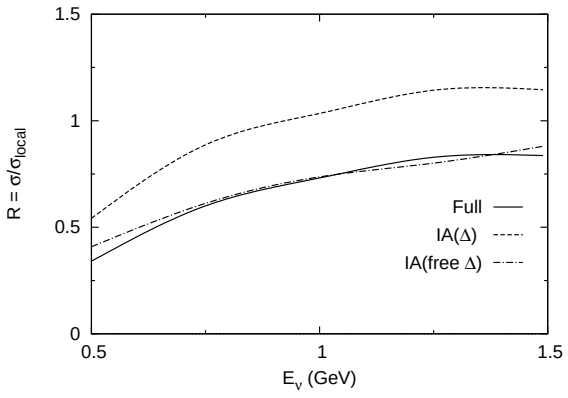

FIG. 10: The effect of the non-locality of the Δ-propagation for $\nu_\mu + {}^{12}\mathrm{C}_{g.s.} \to \mu^- + \pi^+ + {}^{12}\mathrm{C}_{g.s.}$. The ratio $\mathcal{R}$ of the total cross sections obtained with and without taking account of the non-local effect.

mechanism responsible for the axial-vector dominance in the neutrino process works for the photo process in such a manner that coherent photo-pion production is strongly suppressed. Also, the inelastic transition form factor has a peak at a non-zero momentum transfer. As a result, for the photo reaction, the contributions from the incoherent processes become comparable to those from the coherent process. Thus the importance of the incoherent processes relative to the coherent process can be very different between the photo and neutrino processes. Takaki et al. [43] used a similar argument to explain a significant (very small) contribution from the incoherent processes in the photo-pion production (pion-nucleus scattering), compared to the coherent process. This argument may serve as a justification for the assumption currently used in data analyses that the incoherent processes need not be taken into account explicitly .

Finally, we examine the effect of the non-locality of Δ-propagation in nuclei; because we employed the local density approximation for evaluating the Δ Green function [Eq. (17)], this effect arises only from the Δ kinetic term in the Δ Hamiltonian [Eq. (25)]. Although, as mentioned in the introduction, this subject has been studied in Ref. [20], that study only included the Δ-mechanism without considering FSI or the medium effects on the Δ. It is thus interesting to revisit this problem in the framework of our significantly extended treatment. In the local approximation, we neglect the kinetic term in the Δ-Hamiltonian [Eq. (25)], which means that the Δ is considered to be so heavy that it does not propagate in nuclear medium. To facilitate our discussion, we introduce the ratio $\mathcal{R}(E_\nu)$ defined by

$$\mathcal{R}(E_\nu) \equiv \sigma(E_\nu)/\sigma_{\mathrm{local}}(E_\nu)\,, \tag{68}$$

where $\sigma(E_\nu)$ represents the total cross section for $\nu_\mu + {}^{12}\mathrm{C}_{g.s.} \to \mu^- + \pi^+ + {}^{12}\mathrm{C}_{g.s.}$ calculated

with the Δ-propagator including the Δ kinetic term, whereas $\sigma_{\rm local}(E_\nu)$ is that obtained in the local approximation. Figure 10 shows $\mathcal{R}(E_\nu)$ calculated for the various cases. The long-dash curve corresponds to the Δ-only case (without FSI or the medium effects on the Δ; see footnote 5) and the solid line to the case that includes the non-resonant components, medium effects on the Δ and FSI. To make comparison with Ref. [20], we first consider the long-dash line; $\mathcal{R}(E_\nu)$ in this case is found to be 0.55, 1.03 and 1.14 at $E_\nu = 0.5$, 1.0 and 1.5 GeV. Meanwhile, Ref. [20] reports $\mathcal{R}(E_\nu) = \lesssim 0.5$, 0.6 and $\lesssim 1$ at $E_\nu = 0.5$, 1.0 and 1.5 GeV. Although both calculations indicate that the non-local effects are important, our results are qualitatively different from those of Ref. [20]. This difference originates from different ways of treating the energy in the Δ-propagator. In Ref. [20], the in-medium Δ-propagator is assumed to be the same as the free Δ-propagator, whereas our Δ-propagator [$G_{\Delta h}$, Eq. (17)] is a nuclear many-body operator [24] (with some of the medium effects switched off). To illustrate this point, we include in Fig. 10 (dash-dotted line) the results obtained with the use of the free Δ-propagator. In this case, we find $\mathcal{R}(E_\nu) = 0.4$, 0.76 and 0.88 at $E_\nu = 0.5$, 1.0 and 1.5 GeV, which is fairly close to the results in Ref. [20]. The result shown by the solid line indicates that, after the sophistication of the calculation, the non-locality due to the kinetic term is still important over the entire range of E_ν under consideration. In the previous microscopic calculations for neutrino-induced coherent pion production, the non-locality has not been explicitly taken into account. However, this does not necessarily mean that the earlier results are off by an amount suggested by comparison of the curves in Fig. 10, for it is possible that the non-locality effects are partly included with the use of the spreading potential fitted to observables. In view of the importance of the non-local effect, however, we consider it preferable to take it into account explicitly, rather than include it operationally in the Δ mass shift.

An additional point of interest is that it was reported in Ref. [20] that the non-locality changes the shapes of the differential cross sections. We remark that our results (not shown here) agree with that finding.

D. Comparison with SciBooNE and MiniBooNE data

The SciBooNE collaboration has been pursuing a further analysis of the data on neutrino and anti-neutrino CC coherent pion production, and some preliminary results have appeared in Refs.[5, 44]. These results contain detailed information on the differential observables for the pion and muon, and it seems informative to present our theoretical results in a manner that allows ready comparison with these data. To this end, we need to take into account the muon momentum cut ($p_\mu > 350$ MeV) and the momentum transfer cut ($Q^2_{rec} < 0.1$ GeV^2) adopted in the SciBooNE experiment; Q^2_{rec} has been defined in Eq. (64). The theoretical results we present in the following take account of these cuts unless otherwise

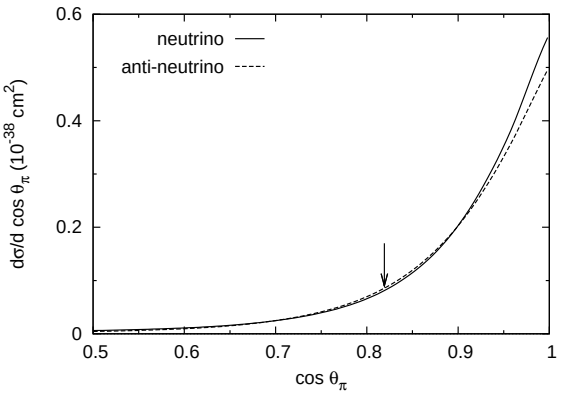

FIG. 11: The $\cos\theta_\pi$-distribution for $\nu_\mu + {}^{12}\mathrm{C}_{g.s.} \to \mu^- + \pi^+ + {}^{12}\mathrm{C}_{g.s.}$ and $\bar{\nu}_\mu + {}^{12}\mathrm{C}_{g.s.} \to \mu^+ + \pi^- + {}^{12}\mathrm{C}_{g.s.}$ at $E_\nu = 1$ GeV. The position of $\theta_\pi = 35^\circ$ is indicated by the arrow.

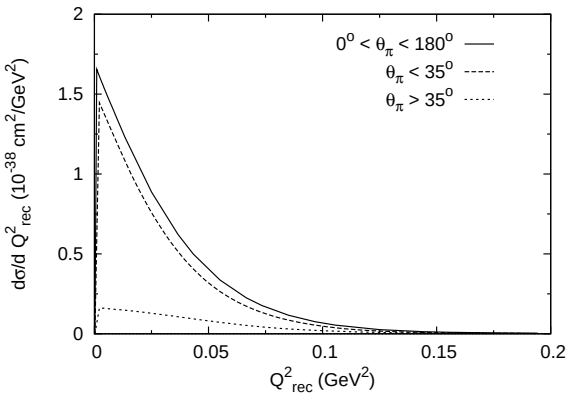

FIG. 12: The $Q^2_{\rm rec}$ distribution for $\nu_\mu + {}^{12}\mathrm{C}_{g.s.} \to \mu^- + \pi^+ + {}^{12}\mathrm{C}_{g.s.}$ at $E_\nu = 1$ GeV.

stated. We will present the results at $E_\nu = 1$ GeV around which the event rate has a peak. Although, for direct comparison, we need to convolute the observables with the (anti-)neutrino flux used in the SciBooNE experiment, the flux has not been released yet. We therefore present our results at a representative value of $E_\nu = 1$ GeV. In Fig. 11, we show the $\cos\theta_\pi$-distribution for the neutrino and anti-neutrino CC processes. In the recent data analysis by the SciBooNE collaboration, events are classified according to the pion emission angle (θ_π). Their preliminary results exhibit a rather clear excess yield for $\theta_\pi < 35^\circ$, which is thought to be ascribable to coherent pion production. In our model, 85% of the pions are emitted in $\theta_\pi < 35^\circ$ for the neutrino CC process at $E_\nu = 1$ GeV, a feature that is in fair agreement with the preliminary SciBooNE result .

Next we show in Fig. 12 (solid line) the $Q^2_{\rm rec}$ distribution for the neutrino reaction.[9] Only the p_μ cut is applied here for an obvious reason. We can see that the contribution from above $Q^2_{\rm rec} = 0.1$ GeV^2 (the value adopted for the $Q^2_{\rm rec}$ cut) constitutes only a small fraction of the entire contribution (3% for the solid curve). The decomposition of the total contribution (solid curve) into two parts according to whether θ_π is smaller or larger than 35° is shown by the dashed curve ($\theta_\pi < 35^\circ$) and the dotted curve ($\theta_\pi > 35^\circ$). The pion and muon momentum distributions are shown in Figs. 13 and 14. The upper (lower) end of the pion (muon) momentum distribution is sharply cut off because of the muon momentum cut ($p_\mu > 350$ MeV). The muon scattering angle distribution is shown in Fig. 15. Figures 11–15 clearly show the characteristics of coherent pion production, i.e., sharply forward scattering (emission) of the muon (pion) with small momentum transfers. Finally, we show

[9] As discussed earlier, the neutrino and anti-neutrino cross sections differ only slightly.

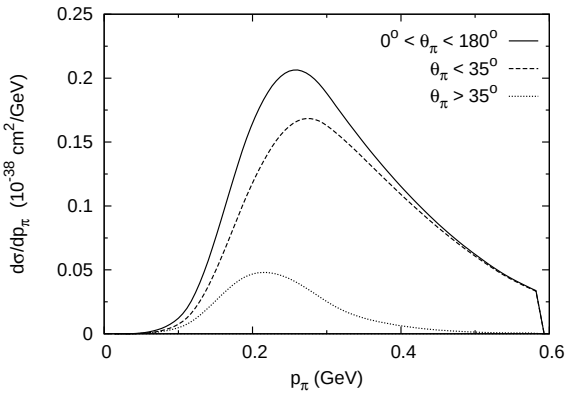

FIG. 13: The pion momentum distribution for $\nu_\mu + {}^{12}\mathrm{C}_{g.s.} \to \mu^- + \pi^+ + {}^{12}\mathrm{C}_{g.s.}$ at $E_\nu = 1$ GeV.

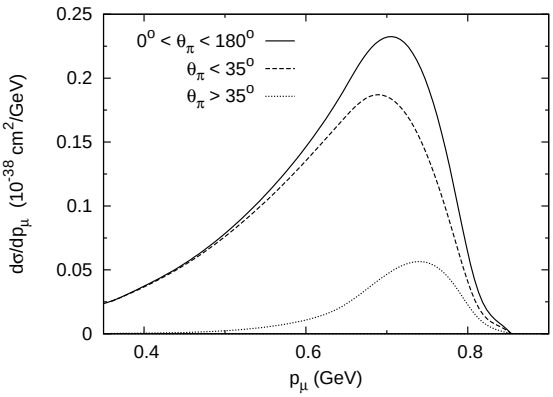

FIG. 14: The muon momentum distribution for $\nu_\mu + {}^{12}\mathrm{C}_{g.s.} \to \mu^- + \pi^+ + {}^{12}\mathrm{C}_{g.s.}$ at $E_\nu = 1$ GeV.

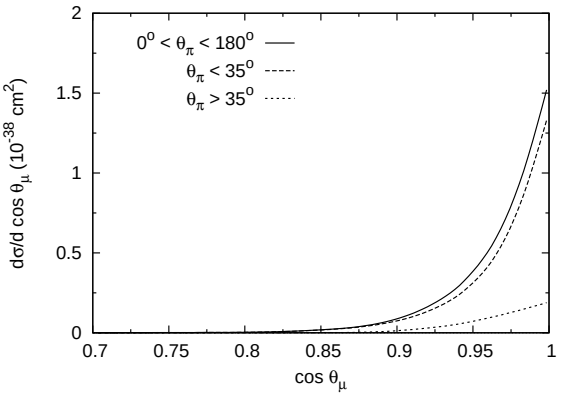

FIG. 15: The muon scattering angle distribution for $\nu_\mu + {}^{12}\mathrm{C}_{g.s.} \to \mu^- + \pi^+ + {}^{12}\mathrm{C}_{g.s.}$ at $E_\nu = 1$ GeV.

in Fig. 16 the spectrum with respect to the coplanar angle difference, $\Delta\phi$, which is defined by $\Delta\phi = \phi_\pi - \pi$, where ϕ_π is the pion azimuthal angle in the LAB frame. (See Fig. 17 for a graphical representation of $\Delta\phi$.) Fig. 16 shows slight asymmetry in the $\Delta\phi$ distribution around $\Delta\phi = 0$. It is interesting to note that this asymmetry is generated mostly by the contribution from the non-resonant amplitudes. To demonstrate this point, we present in the same figure the results obtained with the non-resonant amplitudes turned off, (dash-dotted curve). We also remark that the asymmetry arises mostly from the kinematical region satisfying $\theta_\pi > 35^\circ$ (see the dotted curve). A similar asymmetry also arises for the anti-neutrino process.

The SciBooNE collaboration have recently presented their preliminary results corresponding to Figs. 11–16 for both of the neutrino and anti-neutrino CC coherent pion production

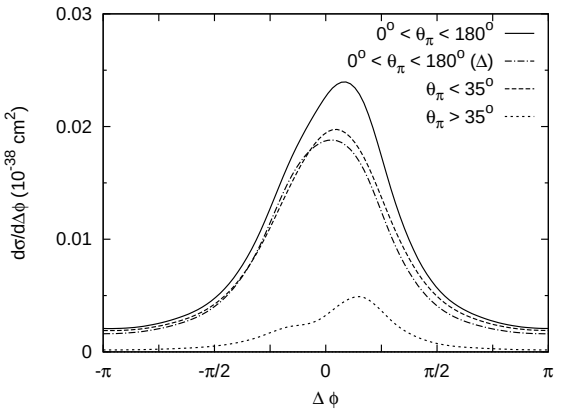

FIG. 16: The coplanar angle difference ($\Delta\phi$) distribution for $\nu_\mu + {}^{12}\mathrm{C}_{g.s.} \to \mu^- + \pi^+ + {}^{12}\mathrm{C}_{g.s.}$ at $E_\nu = 1$ GeV. The definition of $\Delta\phi$ is given in Fig. 17.

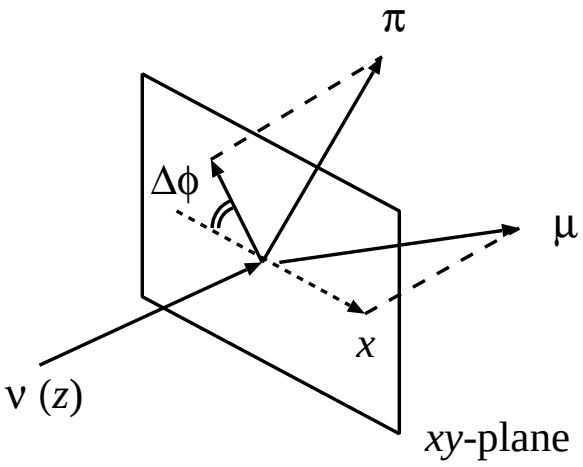

FIG. 17: Graphical definition for the coplanar angle difference ($\Delta\phi$).

reactions [5, 44]. When the flux prediction for the SciBooNE experiment becomes available, we will be able to convolute the results of our calculation with the flux and make direct comparison with the data.

Meanwhile, the MiniBooNE collaboration has been investigating the NC process in (anti-)neutrino-nucleus scattering, and some results for the neutrino process have been published [3], and more results are expected to be released. Since the neutrino flux information for the MiniBooNE experiment is available [40], we can give the theoretical values of relevant observables convoluted with the flux. At present, data are publicly available only for the η-distribution [$\eta \equiv E_\pi(1 - \cos\theta_\pi)$], and we compare our calculation for this quantity with the data. In the analysis of the MiniBooNE NC data, the η-distribution was used to distinguish coherent pion production from other processes contributing to the π^0-production events. To be more specific, MiniBooNE used the "shape" of the η-distribution obtained from the RS model [6] with the momentum reweighting function applied. It has been found, however, that a microscopic calculation in Ref. [7] gives an η-distribution appreciably different from that obtained in the RS model, and the authors of Ref. [7] have pointed out that the MiniBooNE might have substantially overestimated the NC events. Figure 18 shows the "average" η-distribution obtained by convoluting the η-distribution given by our present calculation with the MiniBooNE neutrino flux [40]. For comparison, the figure also shows the MiniBooNE Monte Carlo results (*cf.* Fig. 3b of Ref. [3]), arbitrarily rescaled to match the theoretical curve at $\eta = 0.005$ GeV. We remark that the η-distribution we have obtained is fairly close to that given in Ref. [7], because the non-resonant amplitudes do not change the shape of the η-distribution significantly. Therefore, we arrive at the same conclusion as

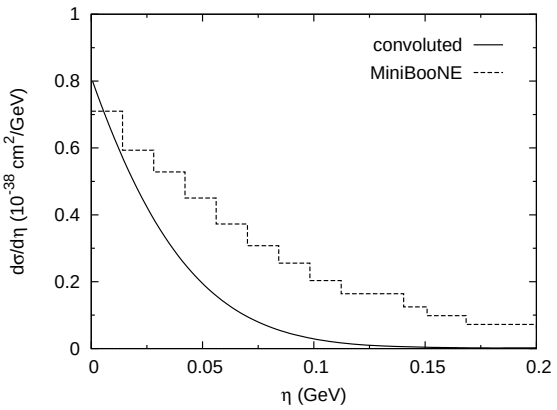

FIG. 18: The flux-convoluted η-distribution for $\nu + {}^{12}\mathrm{C}_{g.s.} \to \nu + \pi^0 + {}^{12}\mathrm{C}_{g.s.}$ obtained in our full calculation. The neutrino flux is taken from MiniBooNE [40]. Also shown is the Monte Carlo result from MiniBooNE [3] rescaled to match our result at $\eta = 0.005$ GeV.

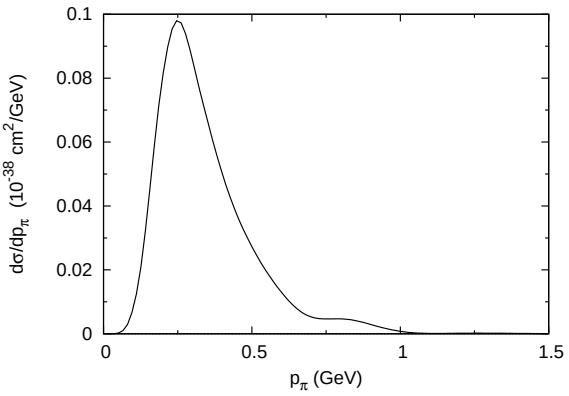

FIG. 19: The flux-convoluted π^0 momentum distribution for $\nu + {}^{12}\mathrm{C}_{g.s.} \to \nu + \pi^0 + {}^{12}\mathrm{C}_{g.s.}$. The neutrino flux is taken from MiniBooNE [40].

in Ref. [7] that it is possible that MiniBooNE substantially overestimated the NC events.

To facilitate a comparison of our calculation with data that are expected to be become available soon from MiniBooNE, we present theoretical predictions for some more quantities that are likely to be relevant. Figure 19 shows the flux-convoluted π^0 momentum distribution predicted by our calculation. As far as observables for the anti-neutrino process are concerned, the flux-convoluted η-distribution resulting from our calculation is given in Fig. 20, and the flux-convoluted π^0 momentum distribution obtained in our model is shown in Fig. 21.

E. Comparison of Microscopic Models

As mentioned, there are mainly two different theoretical approaches to coherent pion production in neutrino-nucleus scattering; a PCAC-based model and a microscopic model. The relation between the RS model (a PCAC-based model) and a microscopic model has been discussed in great detail in Ref. [7], and comparison of those two models, including some improvement of the RS model, has been made in Refs. [7, 8]. The authors of Refs. [7, 8] have emphasized that it can be problematic to use the RS model for $E_\nu \lesssim 2$ GeV. To shed some more light on this issue, we consider it useful to make comparison of different microscopic models. In particular, we focus here on comparison between our model and the model of Amaro et al. [7], which is the most sophisticated among the existing microscopic models for

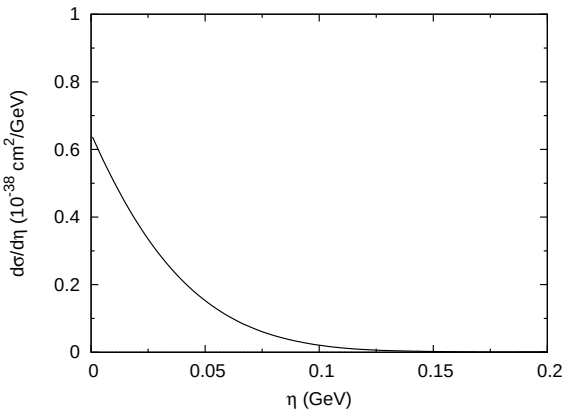

FIG. 20: The flux-convoluted η-distribution for $\bar{\nu} + {}^{12}\mathrm{C}_{g.s.} \to \bar{\nu} + \pi^0 + {}^{12}\mathrm{C}_{g.s.}$. The anti-neutrino flux is taken from MiniBooNE [40].

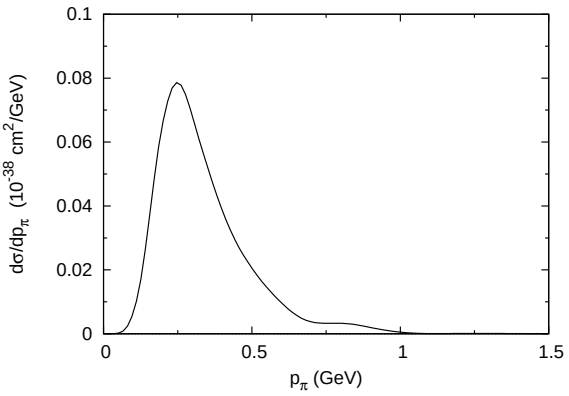

FIG. 21: The flux-convoluted π^0 momentum distribution for $\bar{\nu} + {}^{12}\mathrm{C}_{g.s.} \to \bar{\nu} + \pi^0 + {}^{12}\mathrm{C}_{g.s.}$. The anti-neutrino flux is taken from MiniBooNE [40].

neutrino-induced coherent pion production. [10] The other microscopic calculations in the literature lack one or more aspects that are obviously important, such as the distortion of the final pion and the non-resonant mechanism for the weak currents.

Here, we particularly focus on the elementary amplitudes for pion production off the nucleon. Our approach employs the SL model while Amaro et al. [7] used a model developed in Ref. [46] (to be referred to as HNV). Both SL and HNV include the resonant and non-resonant amplitudes. A point to be noted, however, is that, although both models reproduce reasonably well the data for the $\nu_\mu + N \to \mu^- + \pi^+ + N$ reactions after an appropriate adjustment of the axial-$N\Delta$ coupling, the two models involve rather different reaction mechanisms. In the SL model, we derive a set of tree diagrams from a given Lagrangian with the use of a unitary transformation, and then we embed these tree diagrams in the Lippmann-Schwinger equation, which is solved exactly to yield a non-perturbative pion production amplitude that satisfies π-N two-body unitarity. In HNV, on the other hand, a set of tree diagrams are calculated from a chiral Lagrangian. Then the sum of the contributions of these tree diagrams is identified with the pion production amplitude. At the tree level, the SL and the HNV models have essentially the same non-resonant mechanisms; a contact vertex in HNV may be interpreted as the vector meson exchange mechanism in SL. However the role of the non-resonant amplitude appears differently in the two models. In the SL model, non-resonant amplitude contributes constructively (destructively) to the

[10] A rather extensive comparison of numerical results from various calculations for the neutrino-induced coherent pion production, including those of Amaro et al. [7], recent PCAC-based models [11, 12] and ours, has been presented at NuInt09 by Boyd et al. [45].

resonant amplitudes below (above) the resonance energy. For $\nu_\mu + p \to \mu^- + \pi^+ + p$, the interference of the non-resonant amplitude with the resonant amplitude changes in the SL model the total cross sections by a factor of 1.5, 1.02, 0.96 at $E_\nu = 0.5$, 1, 1.5 GeV [11], while the interference in the HNV always enhances the total cross sections; e.g., enhancement of a factor of 1.1 at $E_\nu = 1.5$ GeV. The difference of the non-resonant mechanism appears also in the coherent pion production on ^{12}C, where only the spin and isospin non-flip amplitude contributes. Whereas the non-resonant amplitude plays an important role in our model (as seen in Figs. 5 and 6), it plays essentially no role in the HNV model. In the neutrino CC coherent pion production, the full (tree) non-resonant amplitude increases the total cross section by 36% (19%) at $E_\nu = 0.5$ GeV and 18% (0.4%) at $E_\nu = 1$ GeV in our model. Thus the non-resonant mechanism in the spin-isospin non-flip amplitude is enhanced by the rescattering process. In the SL model, the non-resonant and resonant πN dynamics in the Δ resonance region has been tested using the extensive data of (γ, π) and $(e, e'\pi)$ reactions. Although the SL model, which provides a unified description of the electroweak pion production reactions, describes very well the available data of the $(\nu, \ell\pi)$ processes, the current data do not yet allow to test the details of the reaction mechanism.

Furthermore, utilizing the consistency of $(\nu, \ell\pi)$, $(e, e'\pi)$ and (π, π) reactions in the SL model, we have developed a model which treats photo- and neutrino-induced coherent pion production processes in a unified manner. Thus we were able to calibrate the reliability of our approach with data for the photo-processes, which is an aspect specific to our approach.

IV. CONCLUSIONS

We have developed a microscopic dynamical model for describing neutrino-induced coherent pion production on nuclei. Because experimental data for neutrino (both elementary and nuclear) processes are rather limited, it is not straightforward to assess the reliability of theoretical calculations. A reasonable strategy to take seems to develop a model which describes strong and electroweak processes in a unified way, and then to test the model extensively by comparing with a large collection of data for the strong-interaction and photo-induced processes and with limited available data for weak processes. We have carried out this program here for the case of the neutrino-induced coherent pion production process. By virtue of the mentioned strategy, our model is probably the most extensively tested one among the existing models for this process. To achieve the stated goal, we need a theoretical framework that provides a unified description for the elementary (π, π'), (γ, π) and $(\nu, \ell\pi)$ processes on a single nucleon. We have adopted the SL model, which is known to give satisfactory descriptions of these elementary amplitudes. We then have combined

[11] See footnote 6.

the SL model with the Δ-hole model to construct a theoretical framework that can describe in a unified way pion-nucleus scattering and electroweak coherent pion production. The unified nature of this approach allows us to fix free parameters in the model using the data for pion-nucleus scattering, which in turn enables us to make parameter-free predictions on electroweak coherent pion production off a nucleus. Another benefit of the present unified approach is that we can assess the reliability of our model by comparing the results for coherent pion photo-production with data. Our model is found to describe reasonably well both pion-nucleus scattering and coherent photo-processes, which establishes a basis for applying the same model to the neutrino-induced processes.

Comparing our numerical results with the recent data on neutrino-induced coherent pion production, we have found that the result for the CC process is consistent with the upper limit from K2K[1], and that the result for the NC process is somewhat smaller than the preliminary experimental value from MiniBooNE[41]. However, as discussed in the literature, MiniBooNE's analysis may have overestimated the cross section due to the use of the RS model in their analysis. We have examined to what extent the various aspects of physics involved in our model individually affect the cross sections. We have shown that the medium effect on the Δ (the spreading potential effect in particular) and the FSI change the cross sections significantly. It is to be noted, however, that these rather drastic changes in the cross sections due to the medium effects are well under control because: (i) the spreading potential and the pion distorted wave function have been fitted to and tested by the empirical total and elastic cross sections for pion-nucleus scattering in and around the Δ region; (ii) the medium effects of a similar magnitude for the photo-process have been shown to bring our calculation into good agreement with the data.

An interesting feature of our model is that the unitarized non-resonant amplitudes give a significant contribution to the cross sections. This is in sharp contrast with the results of the previous calculations; for instance, the calculations in Refs. [7, 15], which considered a tree-level non-resonant mechanism, found almost no contribution from it. It is worth emphasizing that this noticeable difference should not be taken as a measure of uncontrollable model dependence because (as we confirmed) the difference arises largely from unitarization of the non-resonant amplitude, which clearly needs to be implemented.

We have reexamined the non-local effect in Δ-propagation in nuclei. It was emphasized in Ref. [20] that this non-local effect, despite its large size, was not considered explicitly in any of the existing models for neutrino-induced coherent pion production (whether based on a microscopic model or the RS model). The authors of Ref. [20] made this remark based on their calculation that only included the Δ mechanism. Our present calculation, which additionally incorporates the spreading potential and FSI, also indicates that the non-locality gives a large effect. Thus, regardless of the level of sophistication in the treatment of medium effects, one should always include the non-locality effect explicitly.

Because it is expected that the SciBooNE and the MiniBooNE collaborations will report more detailed data on (anti)neutrino-induced coherent CC and NC pion productions, we have presented numerical results relevant to these experiments.

Finally, we made a comparison of the elementary amplitude (HNV[46]) used by Amaro et al.[7] and ours (SL [16, 17]) to clarify similarities and differences between them. The noteworthy points are: (i) At tree-level, both SL and HNV have essentially the same non-resonant mechanism; (ii) In the SL model, a unitary pion-production amplitude is obtained by solving the Lippmann-Schwinger equation in which the tree-diagrams are embedded, whereas, in the HNV model, the sum of the tree-diagrams are identified with the pion-production amplitude; (iii) The non-resonant amplitudes of SL and HNV work differently both for the elementary processes (e.g., $\nu_\mu + p \to \mu^- + \pi^+ + p$), and for coherent pion production; (iv) In SL, the rescattering contribution contained in the non-resonant amplitude considerably enhances the cross section for coherent pion production.

Acknowledgments

S. X. N. acknowledges informative discussions with Hidekazu Tanaka and Hirohisa Tanaka about the SciBooNE and MiniBooNE experiments. S. X. N. also thanks Akira Konaka and Issei Kato for stimulating discussions. This work is supported by the Natural Sciences and Engineering Research Council of Canada and Universidade de São Paulo (SXN), by the U.S. Department of Energy, Office of Nuclear Physics, under contract DE-AC02-06CH11357 (TSHL), by the Japan Society for the Promotion of Science, Grant-in-Aid for Scientific Research(C) 20540270 (TS), and by the U.S. National Science Foundation under contract PHY-0758114 (KK).

APPENDIX A: MULTIPOLE AMPLITUDES

The amplitudes F_i^V, F_i^A in Eqs. (4) and (5) are expressed in terms of multipole amplitudes $E_{l\pm}^{V,A}, M_{l\pm}^{V,A}, S_{l\pm}^{V,A}$ and $L_{l\pm}^A$ as

$$F_1^V = \sum_l [P'_{l+1}E_{l+}^V + P'_{l-1}E_{l-}^V + lP'_{l+1}M_{l+}^V + (l+1)P'_{l-1}M_{l-}^V]\,, \tag{A1}$$

$$F_2^V = \sum_l [(l+1)P'_l M_{l+}^V + lP'_l M_{l-}^V]\,, \tag{A2}$$

$$F_3^V = \sum_l [P''_{l+1}E_{l+}^V + P''_{l-1}E_{l-}^V - P''_{l+1}M_{l+}^V + P''_{l-1}M_{l-}^V]\,, \tag{A3}$$

$$F_4^V = \sum_l [-P''_l E_{l+}^V - P''_l E_{l-}^V + P''_l M_{l+}^V - P''_l M_{l-}^V]\,, \tag{A4}$$

$$F_5^V = \sum_l [(l+1)P'_{l+1}L_{l+}^V - lP'_{l-1}L_{l-}^V]\,, \tag{A5}$$

$$F_6^V = \sum_l [-(l+1)P'_l L^V_{l+} + lP'_l L^V_{l-}]\,, \tag{A6}$$

$$F_7^V = \sum_l [-(l+1)P'_l S^V_{l+} + lP'_l S^V_{l-}]\,, \tag{A7}$$

$$F_8^V = \sum_l [(l+1)P'_{l+1} S^V_{l+} - lP'_{l-1} S^V_{l-}]\,, \tag{A8}$$

and

$$F_1^A = \sum_l [P'_l E^A_{l+} + P'_l E^A_{l-} + (l+2)P'_l M^A_{l+} + (l-1)P'_l M^A_{l-}]\,, \tag{A9}$$

$$F_2^A = \sum_l [(l+1)P'_{l+1} M^A_{l+} + lP'_{l-1} M^A_{l-}]\,, \tag{A10}$$

$$F_3^A = \sum_l [P''_l E^A_{l+} + P''_l E^A_{l-} + P''_l M^A_{l+} - P''_l M^A_{l-}]\,, \tag{A11}$$

$$F_4^A = \sum_l [-P''_{l+1} E^A_{l+} - P''_{l-1} E^A_{l-} - P''_{l+1} M^A_{l+} + P''_{l-1} M^A_{l-}]\,, \tag{A12}$$

$$F_5^A = \sum_l [-(l+1)P'_l L^A_{l+} + lP'_l L^A_{l-}]\,, \tag{A13}$$

$$F_6^A = \sum_l [(l+1)P'_{l+1} L^A_{l+} - lP'_{l-1} L^A_{l-}]\,, \tag{A14}$$

$$F_7^A = \sum_l [(l+1)P'_{l+1} S^A_{l+} - lP'_{l-1} S^A_{l-}]\,, \tag{A15}$$

$$F_8^A = \sum_l [-(l+1)P'_l S^A_{l+} + lP'_l S^A_{l-}]. \tag{A16}$$

$P_L(x)$ is the Legendre function and $x = \hat{k} \cdot \hat{q}$; $\boldsymbol{k}$ and $\boldsymbol{q}$ are the pion momentum and the momentum transfer to the nucleon, respectively.

The multipole amplitudes from isovector currents are further decomposed according to the total isospin (T) in the final πN state as

$$X^{V,A}_{l\pm} = \sum_{T=1/2,3/2} X^{(T)V,A}_{l\pm} \Lambda^T_{ij}\,, \tag{A17}$$

with X being E, M, L or S. We have introduced the projection operator Λ^T_{ij} defined by

$$\Lambda^{3/2}_{ij} = \frac{2\delta_{i,j} - i\epsilon_{ijk}\tau_k}{3} \tag{A18}$$

$$\Lambda^{1/2}_{ij} = \frac{\delta_{i,j} + i\epsilon_{ijk}\tau_k}{3}\,, \tag{A19}$$

where the indexes i and j refer to the final pion isospin state and the component of the isovector current, respectively. For electromagnetic or NC processes, $M^{(0)V}_{l\pm}\tau_i$, which is due to an isoscalar current, is also added to Eq. (A17).

In the main text we sometimes use the notation $X^{V(A),\zeta}_{l\pm}$, where ζ collectively denotes the pion charge and the nucleon isospin state; $X^{V(A),\zeta}_{l\pm}$ is a matrix element (in isospin space) of Eq. (A17). Since we are only concerned with coherent pion production, the specification of the pion charge determines i and j in Eq. (A17). We can find the matrix element (in isospin space) of Eq. (A17) by specifying the nucleon isospin state.

APPENDIX B: LORENTZ TRANSFORMATION FROM ACM TO 2CM

In coherent pion production in neutrino-nucleus scattering ($\nu_\ell + t \to \ell^- + \pi^+ + t$), the elementary process is $W^+(q_A) + N(p_N) \to \pi^+(k_A) + N(p'_N)$, where the four-momenta in the pion-nucleus center-of-mass frame (ACM) are given in the parentheses. We suppose here that the pion momentum is on-shell. In a prescription we employ, the nucleon momenta are fixed as

$$\boldsymbol{p}_N = -\frac{\boldsymbol{q}_A}{A} - \frac{A-1}{2A}(\boldsymbol{q}_A - \boldsymbol{k}_A) \ , \qquad \boldsymbol{p}'_N = -\frac{\boldsymbol{k}_A}{A} + \frac{A-1}{2A}(\boldsymbol{q}_A - \boldsymbol{k}_A) \ , \tag{B1}$$

and the invariant mass (W) of the pion and nucleon is

$$W = \sqrt{(p_N^0 + q_A^0)^2 - (\boldsymbol{p}_N + \boldsymbol{q}_A)^2} \ , \tag{B2}$$

where p_N^0 is the nucleon energy on the mass-shell. We note that W depends on $x_A (\equiv \hat{k}_A \cdot \hat{q}_A)$ as well as $|\boldsymbol{q}_A|$ and $|\boldsymbol{k}_A|$. For convenience, we write $W(|\boldsymbol{q}_A|, |\boldsymbol{k}_A|, x_A)$.

We perform the standard Lorentz transformation from ACM to the πN CM frame (2CM). An arbitrary four-momentum in 2CM (p_2) is written with the corresponding four-momentum in ACM (p_A) as

$$\begin{aligned} \boldsymbol{p}_2 &= \boldsymbol{p}_A - \frac{p_A^0}{W}\boldsymbol{P} + \frac{P^0 - W}{W}(\boldsymbol{p}_A \cdot \hat{P})\hat{P} \ , \\ p_2^0 &= \frac{P^0 p_A^0 - \boldsymbol{p}_A \cdot \boldsymbol{P}}{W} \ , \end{aligned} \tag{B3}$$

with $P = p_N + q_A$.

We now consider a case in which the pion momentum is off-shell (k'_A). We encounter this situation when we consider the final-state interaction in the coherent process. As before, the nucleon momenta are fixed using Eq. (B1) with k_A replaced by k'_A. However, we do not use the nucleon energy on the mass-shell. Instead, we take p_N^0 so that

$$W(|\boldsymbol{q}_A|, |\boldsymbol{k}'_A|, x'_A) = W(|\boldsymbol{q}_A|, |\boldsymbol{k}_A|, x_A) \qquad \text{for } x'_A = x_A \ , \tag{B4}$$

where W is obtained with Eq. (B2). With the nucleon four-momentum (p_N) obtained in this way, we can perform the Lorentz transformation as Eq. (B3). This prescription greatly reduces the amount of labor involved in our numerical calculation, because the SL amplitudes need to be calculated at each value of W. With the variables obtained above, we can calculate Γ_{2AL} used in Eqs. (35) and (42):

$$\Gamma_{2AL} = \sqrt{\frac{\omega'_{\pi,2} p'^0_{N,2} p^0_{N,2}}{\omega'_{\pi,A} p'^0_{N,L} p^0_{N,L}}} \ , \tag{B5}$$

with $\omega'_{\pi,A} = \sqrt{\boldsymbol{k}'^2_A + m_\pi^2}$.

Finally, we discuss the factor Γ^χ,used in Eqs. (35) and (42), which originates from the pion wave function due to the Lorentz transformation. Among the final-state interactions, the simplest process is the scattering of the pion off a single nucleon $\pi(k'_A) + N(p''_N) \to \pi(k_A) + N(p^f_N)$, where the variables in ACM are shown in the parentheses; only k_A is on-shell. Similarly to Eq. (B1), we fix the nucleon momenta as

$$\boldsymbol{p}''_N = -\frac{\boldsymbol{k}'_A}{A} - \frac{A-1}{2A}(\boldsymbol{k}'_A - \boldsymbol{k}_A) \ , \qquad \boldsymbol{p}^f_N = -\frac{\boldsymbol{k}_A}{A} + \frac{A-1}{2A}(\boldsymbol{k}'_A - \boldsymbol{k}_A) \ . \tag{B6}$$

We assume here that the energies of all the nucleons are on the mass-shell. For the Lorentz transformation from ACM to LAB specified this way, we can calculate the Lorentz factor as

$$\Gamma^\chi = \sqrt{\frac{\omega_{\pi,A} E''_{N,A} E^f_{N,A}}{\omega_{\pi,L} E''_{N,L} E^f_{N,L}}} \simeq \sqrt{\frac{\omega_{\pi,A}}{\omega_{\pi,L}}} \ , \tag{B7}$$

Although the actual final-state interaction includes multiple scattering processes, it is beyond our framework to calculate Γ^χ with multiple scattering taken into account. We therefore use Γ^χ calculated for the elementary process in Eqs. (35) and (42). Actually, the Lorentz factor for the plane wave term in Eq. (58) is given by the the rightmost expression in Eq. (B7). Because the approximate equality in Eq. (B7) is quite accurate for $\boldsymbol{k}'_A = \boldsymbol{k}_A$, we use the middle expression in Eq. (B7) to evaluate the matrix elements in Eqs. (35) and (42).

APPENDIX C: EXPRESSIONS FOR SOME COMPONENTS IN THE Δ PROPAGATOR

1. Pauli correction to the Δ self energy

We follow Ref. [25] to calculate the Pauli correction to the Δ self energy ($\Sigma_{\rm Pauli}$). The $\pi N\Delta$ coupling is from the SL model.

$$\begin{aligned} \Sigma_{\rm Pauli} \ &= \ \frac{m_N}{W}\left[2\theta(k_F - \beta) \int_0^{k_F-\beta} dq q^2 \frac{\omega_\pi(q) F^{\rm bare}_{\pi N\Delta}(q) F_{\pi N\Delta}(q)}{K^2 - q^2 + i\epsilon} \right. \\ &+ \ \left. \int_{|k_F-\beta|}^{k_F+\beta} dq q^2 \left(1 - \frac{q^2 + \beta^2 - k_F^2}{2q\beta}\right) \frac{\omega_\pi(q) F^{\rm bare}_{\pi N\Delta}(q) F_{\pi N\Delta}(q)}{K^2 - q^2 + i\epsilon} \right] \ , \end{aligned} \tag{C1}$$

where $\theta(x)$ is the step function, k_F is the Fermi momentum [Eq. (31)], W is the πN invariant mass [Eq. (21)], $\omega_\pi(q) = \sqrt{q^2 + m_\pi^2}$, and

$$K^2 \ = \ \frac{m_N}{W}\left[(W - m_N)^2 - m_\pi^2 \right] \ . \tag{C2}$$

Furthermore, for electroweak pion production amplitude [Eq. (35)],

$$\boldsymbol{\beta} \ = \ \frac{m_N}{W}(\boldsymbol{p}_N + \boldsymbol{q}_A) \ , \tag{C3}$$

where $\boldsymbol{p}_N$ is fixed using Eq. (20), and $\boldsymbol{q}_A$ is the momentum transfer to a nucleus in ACM; for the optical potential [Eq. (52)], $\boldsymbol{q}_A$ is replaced with $\boldsymbol{k}_A$ (the incoming pion momentum). We use the on-shell pion momentum to fix $\boldsymbol{p}_N$. The dressed $\pi N\Delta$ vertex ($F_{\pi N\Delta}$) is taken from Eq. (14), and the bare $\pi N\Delta$ vertex denoted by $F^{\rm bare}_{\pi N\Delta}$ is given as [16]

$$F^{\rm bare}_{\pi N\Delta}(q) = -i\frac{f_{\pi N\Delta}}{m_\pi}\sqrt{\frac{E_N(q)+m_N}{24\pi^2 E_N(q)\omega_\pi(q)}}\left(\frac{\Lambda^2_{\pi N\Delta}}{\Lambda^2_{\pi N\Delta}+q^2}\right)^2 q\ . \tag{C4}$$

2. Δ spreading potential

We consider the following spreading potential consisting of the central and the LS parts:

$$\Sigma_{\rm spr} \ = \ V_C\frac{\rho_t(r)}{\rho_t(0)} + V_{LS}f_{LS}(r)2\boldsymbol{L}_\Delta\cdot\boldsymbol{\Sigma}_\Delta\ , \tag{C5}$$

$$f_{LS}(r) \ = \ \mu r^2 e^{-\mu r^2}\ , \tag{C6}$$

with $\mu = 0.3$ fm^{-2}. We have two complex coupling constants V_C and V_{LS} which are fitted to pion-nucleus scattering data. The radial dependence of the LS spreading potential is taken from Ref. [47]. We implement the spreading potential [Eq. (C5)] in the Δ-propagator after evaluating the doorway state expectation value of the LS term. Thus, the LS term provides an L-dependent shift of the resonance mass and width as[47]

$$\Sigma^L_{LS} = -5V_{LS}\frac{\langle\phi_L|\rho_t f_{LS}k^2 - (\rho_t f_{LS})'\frac{d}{dr} + \frac{L(L+1)}{2r}(\rho_t f_{LS})'\,|\phi_L\rangle}{\langle\phi_L|\rho_t k^2 - (\rho_t)'\frac{d}{dr}|\phi_L\rangle}\ , \tag{C7}$$

with the plane wave pion function $\phi_L(r) = j_L(kr)$.

3. Δ (nucleon) potential

$$V_\Delta(r) = V(r) = (-55\,{\rm MeV})\left(\frac{\rho_t(r)}{\rho_t(0)}\right)\ . \tag{C8}$$

4. Δ Coulomb potential

$$V_\Delta^C(r) = \begin{cases} \frac{2(Z-1)\alpha}{r} , & -\frac{(Z-1)\alpha r^2}{R_e^3} + \frac{3(Z-1)\alpha}{R_e} , & (\pi^+ + p \to \Delta^{++}) \\ \frac{Z\alpha}{r} , & -\frac{Z\alpha r^2}{2R_e^3} + \frac{3Z\alpha}{2R_e} , & (\pi^+ + n \to \Delta^{+}) \\ 0 , & 0 , & (\pi^- + p \to \Delta^{0}) \\ -\frac{Z\alpha}{r} , & \frac{Z\alpha r^2}{2R_e^3} - \frac{3Z\alpha}{2R_e} , & (\pi^- + n \to \Delta^{-}) \end{cases} \quad \begin{matrix} (r \geq R_e) \\ \\ \\ \\ \\ \end{matrix} \quad \begin{matrix} (r < R_e) \\ \\ \\ \\ \\ \end{matrix} \tag{C9}$$

In the above Z is the atomic number. The equivalent square well radius, denoted by R_e, is related to the mean square radius ($\langle r^2 \rangle$) of a nucleus by

$$R_e = \sqrt{\frac{5}{3}\langle r^2 \rangle} . \tag{C10}$$

---

[1] M. Hasegawa et al. [K2K Collaboration], Phys. Rev. Lett. **95**, 252301 (2005).

[2] K. Hiraide et al. [SciBooNE Collaboration], Phys. Rev. D **78**, 112004 (2008).

[3] A. A. Aguilar-Arevalo et al. [MiniBooNE Collaboration], Phys. Lett. **B664**, 41 (2008).

[4] V.T. McGary, Proceedings of 43rd Rencontres de Moriond on Electroweak Interactions and Unified Theories, La Thuile, Italy, 1-8 Mar 2008; arXiv:0806.2347 [hep-ex].

[5] H. Tanaka, proceedings of NUINT09.

[6] D. Rein, L. M. Sehgal, Nucl. Phys. **B223**, 29 (1983).

[7] J.E. Amaro, E. Hernandez, J. Nieves and M. Valverde, Phys. Rev. D **79**, 013002 (2009).

[8] E. Hernández, J. Nieves, M.J. Vicente-Vacas, Phys. Rev. D **80**, 013003 (2009).

[9] P. Vilain et al. [CHARM II Collaboration], Phys. Lett. **B313**, 267 (1993).

[10] D. Rein and L. M. Sehgal, Phys. Lett. **B657**, 207 (2007).

[11] E.A. Paschos, A. Kartavtsev and G.J. Gounaris, Phys. Rev. D **74**, 054007 (2006).

[12] Ch. Berger and L.M. Sehgal, Phys. Rev. D **79**, 053003 (2009).

[13] S. K. Singh, M. S. Athar, S. Ahmad, Phys. Rev. Lett. **96**, 241801 (2006).

[14] L. Alvarez-Ruso, L.S. Geng, S. Hirenzaki, M.J. Vicente Vacas, Phys. Rev. C **75**, 055501 (2007).

[15] L. Alvarez-Ruso, L.S. Geng, M.J. Vicente Vacas, Phys. Rev. C **76**, 068501 (2007).

[16] T. Sato and T.-S. H. Lee, Phys. Rev. C **54**, 2660 (1996).

[17] T. Sato, D. Uno and T.-S. H. Lee, Phys. Rev. C **67**, 065201 (2003).
[18] T. Sato and T.-S. H. Lee, Phys. Rev. C **63**, 055201 (2001).
[19] B. Karaoglu and E. J. Moniz, Phys. Rev. C **33**, 974 (1986).
[20] T. Leitner, U. Mosel, S. Winkelmann, Phys. Rev. C **79**, 057601 (2009).
[21] L. S. Kisslinger, W. L. Wang, Annals Phys. **99**, 374 (1976).
[22] M. Hirata, F. Lenz and K. Yazaki, Annals Phys. **108**, 116 (1977).
[23] M. Hirata, J.H. Koch, E. J. Moniz, and F. Lenz, Annals Phys. **120**, 205 (1979).
[24] S. Taniguchi, T. Sato and H. Ohtsubo, Prog. Theor. Phys. **102**, 333 (1999).
[25] E. J. Moniz and A. Sevgen, Phys. Rev. C **24**, 224 (1981).
[26] J. H. Koch, E. J. Moniz, Phys. Rev. C **20**, 235 (1979); **27**, 751 (1983).
[27] M. Gmitro and J. Kvasil and R. Mach, Phys. Rev. C **31**, 1349 (1985).
[28] A. A. Chumbalov, R. A. Eramzhian and S.S. Kamalov, Z. Phys. A **328**, 195 (1987).
[29] C. W. De Jager, H. De Vries and D. De Vries, At. Data Nucl. Data Tables **36**, 495 (1987).
[30] P. E. Bosted, Phys. Rev. C **51**, 409 (1995).
[31] R. A. Eisenstein and F. Tabakin, Comput. Phys. Commun. **12**, 237 (1976).
[32] A. Kerman, H. McManus and R. Thaler, Ann. Phys. **8**, 551 (1959).
[33] C. M. Vincent and S. C. Phatak, Phys. Rev. C **10**, 391 (1974).
[34] F. Binon, P. Duteil, J. P. Garron, J. Gorres, L. Hugon, J. P. Peigneux, C. Schmit, M. Spighel and J. P. Stroot, Nucl. Phys. **B17**, 168 (1970).
[35] M. Blecher et al., Phys Rev. C **20**, 1884 (1979).
[36] M. J. Leitch et al., Phys Rev. C **29**, 561 (1984).
[37] R. Gothe et al., Phys. Lett. **B355**, 59 (1995).
[38] B. Krusche et al., Phys. Lett. **B526**, 287 (2002).
[39] M. H. Ahn et al., Phys. Rev. D **74**, 072003 (2006).
[40] A.A. Aguilar-Arevalo et al. [MiniBooNE Collaboration], Phys. Rev. D **79**, 072002 (2009).
[41] J. L. Raaf, PhD thesis, University of Cincinnati, FERMILAB-THESIS-2007-20 (2005).
[42] I. Kato and the K2K and T2K collaborations, Nucl. Phys. Proc. Suppl. **B168**, 199 (2007).
[43] T. Takaki, T. Suzuki and J. H. Koch, Nucl. Phys. **A443**, 570 (1985).
[44] K. Hiraide, proceedings of NUINT09.
[45] S. Boyd, S. Dytman, E. Hernández, J. Sobczyk and R. Tacik, Proceedings for NUINT09 will be published. Many plots are available at http://regie2.phys.uregina.ca/neutrino.
[46] E. Hernández, J. Nieves and M. Valverde, Phys. Rev. D **76**, 033005 (2007).
[47] Y. Horikawa, M. Thies and F. Lenz, Nucl. Phys. **A345**, 386 (1980).